Geophysical Journal International

Geophys. J. Int. (2012) **189,** 1335–1352 doi: 10.1111/j.1365-246X.2011.05349.x

Global 3-D imaging of mantle electrical conductivity based on inversion of observatory *C*-responses—I. An approach and its verification

Alexey Kuvshinov and Alexey Semenov

Institute of Geophysics, ETH Zurich, Switzerland. E-mail: kuvshinov@erdw.ethz.ch

Accepted 2011 December 16. Received 2011 December 11; in original form 2011 July 22

SUMMARY

We present a novel frequency-domain inverse solution to recover the 3-D electrical conductivity distribution in the mantle. The solution is based on analysis of local *C*-responses. It exploits an iterative gradient-type method—limited-memory quasi-Newton method—for minimizing the penalty function consisting of data misfit and regularization terms. The integral equation code is used as a forward engine to calculate responses and data misfit gradients during inversion. An adjoint approach is implemented to compute misfit gradients efficiently. Further improvements in computational load come from parallelizing the scheme with respect to frequencies, and from setting the most time-consuming part of the forward calculations—calculation of Green's tensors—apart from the inversion loop. Convergence, performance, and accuracy of our 3-D inverse solution are demonstrated with a synthetic numerical example. A companion paper applies the strategy set forth here to real data.

Key words: Numerical solutions; Inverse theory; Electrical properties; Geomagnetic induction.

1 INTRODUCTION

There is great interest in the characterization of the 3-D properties of the Earth's mantle on a global scale. One technique that has reached a level of maturity is seismic tomography from which 3-D variations in mantle seismic wave speed are recovered (Panning & Romanovicz 2006; Kustowski *et al.* 2008, among others). This information is crucial in characterizing the dynamics of the mantle. For example, geodynamic processes such as mantle convection, the fate of subducting slabs and the origin of continents all have signatures in seismic wave speed. Although seismic tomography has proven important as a means of mapping mantle velocity heterogeneities, it suffers from the inability to separate effects arising from compositional and thermal variations (e.g. Trampert *et al.* 2004; Khan *et al.* 2009). In this context global 3-D electromagnetic (EM) studies, by recovering the 3-D electrical conductivity distribution in the mantle, provide independent and complementary information about the Earth's interior. This is indeed an important issue because conductivity reflects the connectivity of constituents as fluids, partial melt and volatiles (all of which may have profound effects on rheology and, ultimately, mantle convection and tectonic activity), while seismology mostly ascertains bulk mechanical properties.

However, it is only recently that the improvements in global 3-D EM forward modelling (see review paper of Kuvshinov 2008, that summarizes recent progress in this field) and the growth of computational resources have made rigorous 3-D EM inversion on a global scale tractable. A few global and semi-global inverse 3-D solutions have been developed recently (Koyama 2001; Kelbert *et al.* 2008; Tarits & Mandea 2010) providing the first 3-D mantle conductivity models (Fukao *et al.* 2004; Koyama *et al.* 2006; Kelbert *et al.* 2009; Utada *et al.* 2009; Shimizu *et al.* 2010; Tarits & Mandea 2010).

Here, we present an alternative 3-D inverse solution for global induction studies. It is based on the regularized least-squares formulation and exploits a limited-memory quasi-Newton (LMQN) method to solve this optimization problem. As for most other types of optimization methods, the LMQN method requires multiple calculations of the gradient of the data misfit with respect to model parameters. We implemented an adjoint method (Newman & Alumbaugh 2000; Rodi & Mackie 2000; Kelbert *et al.* 2008; Avdeev & Avdeeva 2009; Pankratov & Kuvshinov 2010a, among others) for fast calculation of this gradient. We use the integral equation (IE) modelling code (Kuvshinov *et al.* 2002; Kuvshinov 2008) for the step comprising the forward calculations. In our inversion, the Earth's mantle is parametrized in terms of unknown log conductivities in volume cells of the inversion domain. In this paper, we discuss the details of the global 3-D inversion setup and present the results based on inversion of a synthetic data set. Details of the derivation and calculation of tensor Green's functions of Maxwell's equations for radially varying conductivity distribution are given in Appendices. Note that these tensors are the corner stones of integral equation solution in spherical geometry. The companion paper of Semenov & Kuvshinov (2012) reports the application of the inverse approach to experimental data.

2 INVERSE PROBLEM APPROACH

2.1 Formulation

We formulate the inverse problem of conductivity recovery as an optimization problem such that

$$\phi(\mathbf{m}, \lambda) \underset{\mathbf{m}}{\rightarrow} \min, \tag{1}$$

with the penalty function

$$\phi(\mathbf{m}, \lambda) = \phi_d(\mathbf{m}) + \lambda \phi_s(\mathbf{m}). \tag{2}$$

Here $\phi_d(\mathbf{m})$ is the data misfit

$$\phi_d(\mathbf{m}) = \sum_{\omega \in \Omega} \sum_{\mathbf{r}_a \in Sites} \frac{|C^{\rm mod}(\mathbf{r}_a, \omega, \mathbf{m}) - C^{\rm exp}(\mathbf{r}_a, \omega)|^2}{(\delta C^{\rm exp}(\mathbf{r}_a, \omega))^2}, \tag{3}$$

and λ and $\phi_s(\mathbf{m})$ are a regularization parameter and a regularization term, respectively. $C^{\rm mod}(\mathbf{r}_a, \omega, \mathbf{m})$ and $C^{\rm exp}(\mathbf{r}_a, \omega)$ are (complex-valued) predicted and observed C-responses at observation site $\mathbf{r}_a$ and at frequency ω (see the definition of the C-responses in Section 2.2), and $\delta C^{\rm exp}(\mathbf{r}_a, \omega)$ are the uncertainties of the observed responses. 'Sites' define the locations of the geomagnetic observatories

$$\text{Sites} := \{(r = a, \vartheta_i, \varphi_i), i = 1, 2, \ldots, N_{\rm sites}\}, \tag{4}$$

where $a = 6371.2$ km is the mean radius of the Earth, ϑ_i and φ_i are respectively colatitude and longitude of the observation site. 'Ω' define the frequencies under consideration

$$\Omega := \{\omega_k, k = 1, 2, \ldots, N_{\rm freq}\}. \tag{5}$$

Vector $\mathbf{m}$ represents the model parameters that describe the 3-D conductivity distribution in the model. Parametrization of the model is explained in Section 2.4.

We work with a regularization term of the form

$$\phi_s(\mathbf{m}) = \{W\mathbf{m}\}^{\rm T}\{W\mathbf{m}\}, \tag{6}$$

where the superscript T means transpose and W presents a regularization matrix which—together with the regularization parameter λ—controls the model smoothness. As a smoothing matrix the finite difference approximation to the gradient operator is used.

2.2 C-responses

If the source can be represented via a first zonal harmonic, $P_1^0 = \cos\vartheta_d$, in geomagnetic coordinates (this is our case since we work with magnetospheric ring current as a source), and if the Earth is assumed to be regionally 1-D, then the so-called C-response can be introduced at a given site, $\mathbf{r}_a \in$ Sites, and at a given frequency, ω, as (Banks 1969)

$$C(\omega, \mathbf{r}_a) = -\frac{a \tan\vartheta_d}{2} \frac{H_r(\mathbf{r}_a, \omega)}{H_{\vartheta_d}(\mathbf{r}_a, \omega)}, \tag{7}$$

where ϑ_d is the geomagnetic colatitude of the observation site, H_r and H_{ϑ_d} are respectively the radial and horizontal (directed toward geomagnetic south) components of the magnetic field. The complex-valued C-response has physical dimension of length, and its real part provides an estimation of the depth to which EM field penetrates (Weidelt 1972). This technique of estimating (and then interpreting) C-responses is referred to as the geomagnetic depth sounding (GDS) method. There is a common consensus that GDS works fairly well in a period range between a few days and a few months (Banks 1969; Roberts 1984; Schultz 1987; Fujii & Schultz 2002, among others), thus allowing for the recovery of electrical conductivities in the depth range from 400–500 km down to 1600 km.

2.3 Calculation of C-responses in a 3-D conductivity model

As it is seen from eq. (7) the calculation of the responses relies on a prediction of the frequency-domain magnetic field $\mathbf{H}$ at $\mathbf{r}_a \in$ Sites in a given spherical 3-D conductivity model of the Earth which is induced by a given source $\mathbf{j}^{\rm ext}(\mathbf{r})$. The magnetic and electric fields, $\mathbf{H}$ and $\mathbf{E}$, in such a model obey Maxwell's equations

$$\nabla \times \mathbf{H}(\mathbf{r}) = \sigma(\mathbf{r})\mathbf{E}(\mathbf{r}) + \mathbf{j}^{\rm ext}(\mathbf{r}), \tag{8}$$

$$\nabla \times \mathbf{E}(\mathbf{r}) = {\rm i}\omega\mu_0\mathbf{H}(\mathbf{r}), \tag{9}$$

where $\mathbf{r} = (r, \vartheta, \varphi)$, μ_0 is the magnetic permeability of the free space, $\omega = 2\pi/T$—angular frequency, T—period, and $\sigma(\mathbf{r})$ is the 3-D conductivity distribution in the model. Here we assume that the time factor is $e^{-{\rm i}\omega t}$. We solve eqs (8)–(9) using the integral equation approach which is based on a contraction operator (Pankratov *et al.* 1995; Singer 1995; Singer 2008, among others). Displacement currents are ignored in the considered period range. The 3-D numerical solution based on this approach has already been successfully applied for a variety of global induction studies (*cf.* Kuvshinov 2008). Here we shortly outline the key ideas of the approach/solution, since they are important for understanding the scheme by which the inverse solver is made computationally more efficient, which is described in Section 4.1.

We start by introducing a 'reference' radially symmetric (1-D) model of conductivity $\sigma_0(r)$. The reference magnetic and electric fields, $\mathbf{H}^0$ and $\mathbf{E}^0$, of this model obey Maxwell's equations

$$\nabla \times \mathbf{H}^0(\mathbf{r}) = \sigma_0(r)\mathbf{E}^0(\mathbf{r}) + \mathbf{j}^{\rm ext}(\mathbf{r}), \tag{10}$$

$$\nabla \times \mathbf{E}^0(\mathbf{r}) = {\rm i}\omega\mu_0\mathbf{H}^0(\mathbf{r}). \tag{11}$$

If we are able to construct and calculate fundamental solutions ('current-to-electric', $G^{ej}_{\rm 1D}$, and 'current-to-magnetic', $G^{hj}_{\rm 1D}$, tensor Green's functions) of eqs (10)–(11), then $\mathbf{H}^0$ and $\mathbf{E}^0$ can be determined via convolution integrals

$$\mathbf{H}^0(\mathbf{r}) = \int_{V^{\rm ext}} G^{hj}_{\rm 1D}(\mathbf{r}, \mathbf{r}')\mathbf{j}^{\rm ext}(\mathbf{r}')\, {\rm d}v', \tag{12}$$

$$\mathbf{E}^0(\mathbf{r}) = \int_{V^{\rm ext}} G^{ej}_{\rm 1D}(\mathbf{r}, \mathbf{r}')\mathbf{j}^{\rm ext}(\mathbf{r}')\, {\rm d}v'. \tag{13}$$

Here $\mathbf{r} \in \mathbb{R}^3$, $\mathbf{r}' \in V^{\rm ext}$, and $V^{\rm ext}$ is the volume occupied by $\mathbf{j}^{\rm ext}$. Note that in all quantities discussed (except conductivities) the dependence on ω is implicit, but omitted for the simplicity of presentation. We assume that $G^{ej}_{\rm 1D}$ and $G^{hj}_{\rm 1D}$ are known. The subscript '1D' means that Green's functions depend not only on $\mathbf{r}$, $\mathbf{r}'$ and ω but also depend on the 1-D conductivity distribution $\sigma_0(r)$. A formalism for the derivation and calculation of these tensors is presented in Appendices A–F of this paper.

Introducing further 'scattered' fields, $\mathbf{E}^{\rm s} = \mathbf{E} - \mathbf{E}^0$ and $\mathbf{H}^{\rm s} = \mathbf{H} - \mathbf{H}^0$ and subtracting eqs (10)–(11) from eqs (8)–(9), one can write Maxwell's equations for scattered fields in the following form

$$\nabla \times \mathbf{H}^{\rm s}(\mathbf{r}) = \sigma_0(r)\mathbf{E}^{\rm s}(\mathbf{r}) + \mathbf{j}^q(\mathbf{r}), \tag{14}$$

$$\nabla \times \mathbf{E}^{\rm s}(\mathbf{r}) = {\rm i}\omega\mu_0\mathbf{H}^{\rm s}(\mathbf{r}), \tag{15}$$

where

$$\mathbf{j}^q(\mathbf{r}) = \big[\sigma(\mathbf{r}) - \sigma_0(r)\big]\mathbf{E}^{\rm s}(\mathbf{r}) + \mathbf{j}^{\rm s}(\mathbf{r}), \tag{16}$$

and

$$\mathbf{j}^{\rm s}(\mathbf{r}) = \big[\sigma(\mathbf{r}) - \sigma_0(r)\big]\mathbf{E}^0(\mathbf{r}). \tag{17}$$

Comparing eqs (10)–(11) and eqs (14)–(15) one can deduce that the scattered magnetic and electric fields, $\mathbf{H}^{\rm s}$ and $\mathbf{E}^{\rm s}$, in analogy with eqs (12) and (13) can be written as

$$\mathbf{H}^{\rm s}(\mathbf{r}) = \int_{V^{\rm mod}} G^{hj}_{\rm 1D}(\mathbf{r}, \mathbf{r}')\mathbf{j}^q(\mathbf{r}')\, {\rm d}v', \tag{18}$$

$$\mathbf{E}^{\rm s}(\mathbf{r}) = \int_{V^{\rm mod}} G^{ej}_{\rm 1D}(\mathbf{r}, \mathbf{r}')\mathbf{j}^q(\mathbf{r}')\, {\rm d}v', \tag{19}$$

where $\mathbf{r} \in \mathbb{R}^3$, $\mathbf{r}' \in V^{\rm mod}$, and $V^{\rm mod}$ is a region where $\sigma(\mathbf{r}) - \sigma_0(r)$ differs from 0. If we restrict ourselves to $\mathbf{r} \in V^{\rm mod}$ we obtain from eq. (19) a conventional integral equation with respect to the unknown scattered electric field, $\mathbf{E}^{\rm s}$

$$\mathbf{E}^{\rm s}(\mathbf{r}) - \int_{V^{\rm mod}} G^{ej}_{\rm 1D}(\mathbf{r}, \mathbf{r}')\big[\sigma(\mathbf{r}') - \sigma_0(r')\big]\mathbf{E}^{\rm s}(\mathbf{r}')\, {\rm d}v' = \mathbf{E}_f(\mathbf{r}), \tag{20}$$

where the free term, $\mathbf{E}_f(\mathbf{r})$, is given by

$$\mathbf{E}_f(\mathbf{r}) = \int_{V^{\rm mod}} G^{ej}_{\rm 1D}(\mathbf{r}, \mathbf{r}')\mathbf{j}^{\rm s}(\mathbf{r}')\, {\rm d}v'. \tag{21}$$

After discretization, eq. (20) can be solved iteratively using, for example, one of the conjugate gradient methods (CGM). However, for high-contrasting models the resulting system of linear equations is poorly conditioned which makes the numerical solution of eq. (20) unstable. The remedy to overcome this problem is to modify eq. (20) to an integral equation with contraction operator (*cf.* Pankratov *et al.* 1995)

$$\chi(\mathbf{r}) - \int_{V^{\rm mod}} K(\mathbf{r}, \mathbf{r}')R(\mathbf{r}')\chi(\mathbf{r}')\, {\rm d}v' = \chi_0(\mathbf{r}), \tag{22}$$

where

$$R(\mathbf{r}') = \frac{\sigma(\mathbf{r}') - \sigma_0(r')}{\sigma(\mathbf{r}') + \sigma_0(r')}, \tag{23}$$

$$K(\mathbf{r}, \mathbf{r}') = \delta(\mathbf{r} - \mathbf{r}')I + 2\sqrt{\sigma_0(r)}G^{ej}_{\rm 1D}(\mathbf{r}, \mathbf{r}')\sqrt{\sigma_0(r')}, \tag{24}$$

$$\chi_0(\mathbf{r}) = \int_{V^{\rm mod}} K(\mathbf{r}, \mathbf{r}')\frac{\sqrt{\sigma_0(r')}}{\sigma(\mathbf{r}') + \sigma_0(r')}\mathbf{j}^{\rm s}(\mathbf{r}')\, {\rm d}v', \tag{25}$$

$$\chi(\mathbf{r}') = \frac{1}{2\sqrt{\sigma_0(r')}}\Big\{\big[(\sigma(\mathbf{r}') + \sigma_0(r')\big]\mathbf{E}^{\rm s}(\mathbf{r}') + \mathbf{j}^{\rm s}(\mathbf{r}')\Big\}. \tag{26}$$

Here $\delta(\mathbf{r} - \mathbf{r}')$ is Dirac's delta function and I is the identity matrix. The advantage of this form of integral equation is that after discretization, the resulting system of linear equations appears to be well conditioned even for high-contrasting models. It can thus be efficiently solved by CGM. The specific form of eq. (22) is motivated by the energy inequality for the scattered EM field, which expresses a fundamental physical fact that the energy flow of the scattered field outside the domain with inhomogeneities is always non-negative (*cf.* Singer 1995; Pankratov *et al.* 1995).

At this stage it is important to remark that eqs (12) and (13) are valid for any distribution of the impressed current at any location. However, since we deal here with the responses generated by the source, which is usually considered in the form of spherical harmonic expansion (SHE) of the equivalent sheet current (see Appendix G), general expressions for $\mathbf{H}^0$ and $\mathbf{E}^0$ in eqs (12) and (13) will also appear in the form of a SHE. This is explained further in Appendix H.

A 3-D IE forward modelling solution that provides C-response predictions can be represented as a sequence of the following steps.

(1) $G^{ej}_{\rm 1D}(\mathbf{r}, \mathbf{r}')$ and then $K(\mathbf{r}, \mathbf{r}')$ (eq. 24) are calculated for $\mathbf{r}, \mathbf{r}' \in V^{\rm mod}$;
(2) $G^{hj}_{\rm 1D}(\mathbf{r}_a, \mathbf{r}')$ is calculated for $\mathbf{r}_a \in$ Sites and $\mathbf{r}' \in V^{\rm mod}$;
(3) $\mathbf{E}^0(\mathbf{r})$ is calculated for $\mathbf{r} \in V^{\rm mod}$ using eqs (H1) and (H2);
(4) $\mathbf{j}^{\rm s}(\mathbf{r})$ is calculated for $\mathbf{r} \in V^{\rm mod}$ using eq. (17) and $\mathbf{E}^0$ from step 3;
(5) $\chi_0(\mathbf{r})$ is calculated for $\mathbf{r} \in V^{\rm mod}$ using eq. (25) with K from step 1;
(6) The scattering eq. (22) is solved on $V^{\rm mod}$ using CGM;
(7) $\mathbf{E}^{\rm s}(\mathbf{r})$ is calculated for $\mathbf{r} \in V^{\rm mod}$ using eq. (26) with $\mathbf{j}^{\rm s}$ from step 4;
(8) $\mathbf{j}^q(\mathbf{r})$ is calculated for $\mathbf{r} \in V^{\rm mod}$ using eq. (16) with $\mathbf{j}^{\rm s}$ from step 4;
(9) $\mathbf{H}^{\rm s}(\mathbf{r}_a)$ is calculated for $\mathbf{r}_a \in$ Sites using eq. (18) with $G^{hj}_{\rm 1D}$ from step 2;
(10) $\mathbf{H}^0(\mathbf{r}_a)$ is calculated for $\mathbf{r}_a \in$ Sites using eqs (H3) and (H4);
(11) $\mathbf{H}(\mathbf{r}_a)$ is calculated for $\mathbf{r}_a \in$ Sites as a sum of $\mathbf{H}^{\rm s}$ and $\mathbf{H}^0$ from steps 9 and 10;
(12) $C^{\rm mod}(\mathbf{r}_a)$ is calculated for $\mathbf{r}_a \in$ Sites using eqs (7) and (33).

Henceforce, this scheme will be referred as the 'IE-C' solution.

2.4 Parametrization of the model

Let $V^{\rm inv}$ be the inversion problem domain where we seek a 3-D conductivity distribution. Also let $V^{\rm mod}$ be the forward problem domain where we solve eqs (8)–(9). We assume that $V^{\rm inv}$ is confined to $N^{\rm inv}_r$ laterally non-uniform spherical layers embedded into the Earth's model, which consists of a surface shell of known laterally varying conductance, $S(\vartheta, \varphi)$ and background 1-D section of known conductivity $\sigma_b(r)$ (see the sketch of 3-D model in Fig. 1). For our problem statement it is important to include the surface shell (which approximates non-uniform distribution of the conducting oceans and resistive continents) into $V^{\rm mod}$, since this shell greatly affects the responses at coastal observatories (Kuvshinov *et al.* 2002). Thus $V^{\rm mod}$ consists of $V^{\rm inv}$ and the thin surface layer. $V^{\rm mod}$ is discretized by $N^{\rm mod} = N^{\rm mod}_r \times N^{\rm mod}_\vartheta \times N^{\rm mod}_\varphi$ volume cells, V_j $(j = 1, 2, \ldots, N^{\rm mod})$, in spherical coordinates (r, ϑ and φ). Here $N^{\rm mod}_r = N^{\rm inv}_r + 1$.

The model parametrization $\mathbf{m}$ is defined as follows. Let $V^{\rm inv}$ be subdivided onto $N^{\rm inv} = N^{\rm inv}_r \times N^{\rm inv}_\tau$ volume cells, V_m $(m = 1, 2, \ldots, N^{\rm inv})$. Here $N^{\rm inv}_\tau$ is a number of cells in horizontal direction. We assume that the conductivity is constant within V_m

$$\sigma(\mathbf{r}) = \sigma_m, \quad \mathbf{r} \in V_m. \tag{27}$$

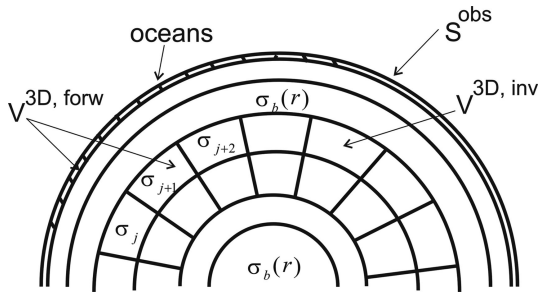

Figure 1. Sketch of 3-D conductivity model.

Then the vector

$$\mathbf{m} = (\ln\sigma_1, \ln\sigma_2, \ldots \ln\sigma_{N^{\rm inv}})^{\rm T}, \tag{28}$$

defines the set of model parameters. The choice of $\ln(\sigma)$ instead of σ as unknowns guarantees that the conductivities are positive during an inversion and provides a better scaling of the problem. We also note that the sizes of the cells along r and ϑ can be variable.

Note that V_m might coincide with V_j within $V^{\rm inv}$, or might be defined by some combinations of V_j. In the present version of the inverse solution only one type of combination of V_j (to comprise V_m) is allowed, namely simultaneous merging in both lateral directions of L^2 cells V_j within each of $N_r^{\rm inv}$ inhomogeneous layers. Thus, for this merging scheme $N_\tau^{\rm inv} = N_\vartheta^{\rm mod}/L \times N_\varphi^{\rm mod}/L$.

2.5 Limited-memory quasi-Newton method

To minimize $\phi(\mathbf{m}, \lambda)$ in eq. (2) we apply the limited-memory quasi-Newton method which has become a popular tool to solve large-scale 3-D EM inverse problems numerically (Haber 2005; Plessix & Mulder 2008; Avdeev & Avdeeva 2009, among others). Our implementation of the method follows Nocedal & Wright (2006). The LMQN method is an iterative method and it is based on the updating the trial solution

$$\mathbf{m}_{k+1} = \mathbf{m}_k + \alpha_k \mathbf{p}_k, \tag{29}$$

where $\mathbf{p}_k$ is determined as

$$\mathbf{p}_k = -B_k^{-1}\nabla\phi_k. \tag{30}$$

Here k is the iteration number, α_k is the step length, B_k^{-1} is an approximation of the inverse Hessian matrix, and

$$\nabla\phi_k = \left(\frac{\partial\phi}{\partial m_1}, \frac{\partial\phi}{\partial m_2}, \ldots, \frac{\partial\phi}{\partial m_{N^{\rm inv}}}\right)^{\rm T}\Bigg|_{\mathbf{m}=\mathbf{m}_k}, \tag{31}$$

is the gradient vector with respect to the current model parameters $\mathbf{m}_k$. Thus the updating procedure requires three basic operations: (1) updating $\nabla\phi_k$; (2) updating B_k^{-1}; and (3) finding the appropriate α_k. B_k^{-1} is efficiently updated using limited-memory Broyden-Fletcher-Goldfarb-Shanno formula and α_k is found by an inexact line search also described in Nocedal & Wright (2006). Computation of $\nabla\phi_k$ requires calculation of misfit gradient, $\nabla\phi_d$, and the gradient of the regularization term, $\nabla\phi_s$ (hereinafter we omit dependence of these quantities on k to simplify presentation). Usually the evaluation of $\nabla\phi_s$ can be done analytically. For example, the gradient of our ϕ_s (see eq. 6) has the form

$$\nabla\phi_s = 2W^{\rm T}W\mathbf{m}. \tag{32}$$

But the calculation of $\nabla\phi_d$ is not so trivial. The straightforward option—brute-force numerical differentiation—is computationally expensive requiring $N^{\rm inv}+1$ forward modellings per LMQN update and frequency. A much more efficient and elegant way to calculate the gradient of the misfit is provided by the so-called 'adjoint' approach. It allows for the calculation of the misfit gradient for the price of only few additional forward modellings excited by a specific (adjoint) source. Each inverse problem setting requires the finding of explicit formulas for the adjoint source. Pankratov & Kuvshinov (2010a) presented a general formalism for the adjoint calculation of the misfit gradients with respect to variations in the 3-D conductivity. Using this formalism one can readily obtain appropriate formulae for the specific frequency-domain sounding method. To illustrate the concept the authors provided these formulae for a number of EM techniques. Section 3.1 gives a summary of their results for the GDS case.

3 EFFICIENT CALCULATION OF THE MISFIT GRADIENT

3.1 Adjoint approach to calculate gradient

Because it is most natural to relate the 3-D conductivity distribution to the geographic coordinate system, all (forward and inverse) calculations are performed in geographic coordinates. Bearing this in mind H_{ϑ_d} in eq. (7) can be rewritten as

$$H_{\vartheta_d}(\mathbf{r}_a, \omega) = \cos\alpha(\mathbf{r}_a)H_\vartheta(\mathbf{r}_a, \omega) - \sin\alpha(\mathbf{r}_a)H_\varphi(\mathbf{r}_a, \omega), \tag{33}$$

where H_ϑ and H_φ are the components directed toward geographic south and east, respectively, and $\alpha(\mathbf{r}_a)$ is the angle between directions to geographic and geomagnetic north at observation site $\mathbf{r}_a$. Following Pankratov & Kuvshinov (2010a) the individual entries of $\nabla\phi_d$ can be calculated from

$$\frac{\partial\phi_d}{\partial m_i} = \frac{2}{\sigma_i}\Re\Big\{\sum_{\omega\in\Omega}\int_{V_i}\big[E_r(\mathbf{r}')E_r^A(\mathbf{r}') + E_\vartheta(\mathbf{r}')E_\vartheta^A(\mathbf{r}') + E_\varphi(\mathbf{r}')E_\varphi^A(\mathbf{r}')\big]{\rm d}v'\Big\}, \tag{34}$$

where $V_i \in V^{\rm inv}$, $i = 1, 2, \ldots, N^{\rm inv}$, $\Re$ stands for the real part, $\mathbf{E}$ is the solution of eqs (8)–(9) and $\mathbf{E}^A$ is the solution of Maxwell's equations

$$\nabla\times\mathbf{H}^A(\mathbf{r}) = \sigma(\mathbf{r})\mathbf{E}^A(\mathbf{r}), \tag{35}$$

$$\nabla\times\mathbf{E}^A(\mathbf{r}) = {\rm i}\omega\mu_0\mathbf{H}^A(\mathbf{r}) + \mathbf{h}(\mathbf{r}), \tag{36}$$

where the adjoint, 'magnetic', source is given by

$$\mathbf{h}(\mathbf{r}) = \sum_{\mathbf{r}_a\in{\rm Sites}}\mathbf{M}(\mathbf{r}_a)\delta(\mathbf{r}-\mathbf{r}_a), \tag{37}$$

with

$$\mathbf{M}(\mathbf{r}) = K\frac{\big[C^{\rm mod}(\mathbf{r},\mathbf{m}) - C^{\rm exp}(\mathbf{r})\big]^*}{\big[\delta C^{\rm exp}(\mathbf{r})\big]^2}\Big\{\frac{1}{H_{\vartheta_d}(\mathbf{r})}\mathbf{e}_r - \frac{H_r(\mathbf{r})}{H_{\vartheta_d}^2(\mathbf{r})} \times\big[\cos\alpha(\mathbf{r})\mathbf{e}_\vartheta - \sin\alpha(\mathbf{r})\mathbf{e}_\varphi\big]\Big\}. \tag{38}$$

Here K denotes $-\frac{a\tan\vartheta_d}{2}$, and superscript '*' stands for the complex conjugation. (Note again that all quantities under discussion depend on the frequency ω). Thus the adjoint source is an array of magnetic dipoles which are located at the observation sites, with the magnitudes determined by the residuals of the responses. The interested readers are referred to the paper of Pankratov & Kuvshinov (2010a) for the details of derivation of eqs (34), (37) and (38). These equations demonstrate the essence of the adjoint approach: to calculate the gradient of the misfit one needs to perform only one (per frequency) additional forward modelling with the excitation provided by the adjoint source. This forward modelling differs from that described in Section 2.3 in the following point: now we have to consider Maxwell's equations for the reference fields with the magnetic source

$$\nabla\times\mathbf{H}^{0,A}(\mathbf{r}) = \sigma_0(r)\mathbf{E}^{0,A}(\mathbf{r}), \tag{39}$$

$$\nabla\times\mathbf{E}^{0,A}(\mathbf{r}) = {\rm i}\omega\mu_0\mathbf{H}^{0,A}(\mathbf{r}) + \mathbf{h}(\mathbf{r}). \tag{40}$$

Then if we are able to construct and calculate fundamental solution ('magnetic-to-electric' tensor Green's function, $G_{\rm 1D}^{eh}$) of eqs (39) and (40), then $\mathbf{E}^{0,A}$ can be represented via the following convolution integral

$$\mathbf{E}^{0,A}(\mathbf{r}) = \int_{V^{\rm ext}} G_{\rm 1D}^{eh}(\mathbf{r},\mathbf{r}')\mathbf{h}(\mathbf{r}')\,{\rm d}v'. \tag{41}$$

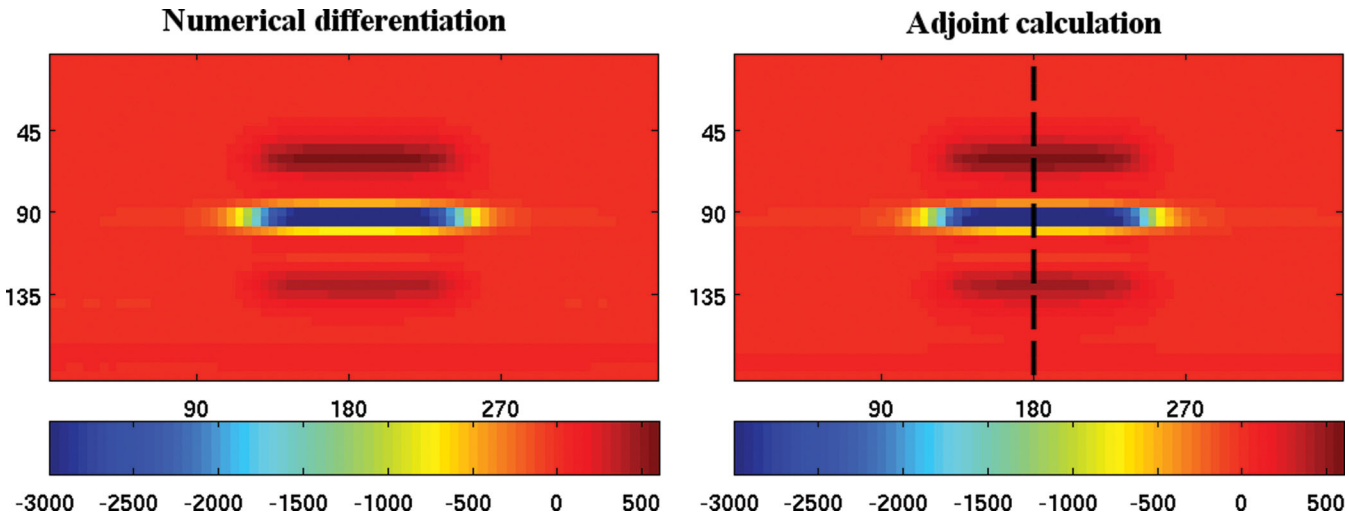

Figure 2. Comparison of the data misfit gradients calculated by adjoint method (right-hand plot) and numerical differentiation (left-hand plot).

Substituting eq. (37) into eq. (41) we obtain for $\mathbf{E}^{0,A}$

$$\mathbf{E}^{0,A}(\mathbf{r}) = \sum_{\mathbf{r}_a \in \text{Sites}} G^{eh}_{1\text{D}}(\mathbf{r}, \mathbf{r}_a)\mathbf{M}(\mathbf{r}_a). \tag{42}$$

With $\mathbf{E}^{0,A}(\mathbf{r})$ at hand we can proceed exactly in the same way as we did in Section 2.3. A 3-D IE forward modelling solution which provides the misfit gradient can be summarized with the following steps

(1) $G^{ej}_{1\text{D}}(\mathbf{r}, \mathbf{r}')$ and then $K(\mathbf{r}, \mathbf{r}')$ (see eq. 24) are calculated for $\mathbf{r}$, $\mathbf{r}' \in V^{\text{mod}}$;
(2) $G^{eh}_{1\text{D}}(\mathbf{r}, \mathbf{r}_a)$ is calculated for $\mathbf{r} \in V^{\text{mod}}$ and $\mathbf{r}_a \in$ Sites;
(3) $\mathbf{E}^{0,A}(\mathbf{r})$ is calculated for $\mathbf{r} \in V^{\text{mod}}$ using eq. (42) with $G^{eh}_{1\text{D}}$ from step 2;
(4) $\mathbf{j}^{s,A}(\mathbf{r})$ is calculated for $\mathbf{r} \in V^{\text{mod}}$ using eq. (17) and $\mathbf{E}^{0,A}$ from step 3;
(5) $\chi_{0,A}(\mathbf{r})$ is calculated for $\mathbf{r} \in V^{\text{mod}}$ using eq. (25) with K from step 1;
(6) the scattering eq. (22) is solved on V^{mod} using CGM;
(7) $\mathbf{E}^{s,A}(\mathbf{r})$ is calculated for $\mathbf{r} \in V^{\text{mod}}$ using eq. (26) and $\mathbf{j}^{s,A}$ from step 4;
(8) $\mathbf{E}^{A}(\mathbf{r})$ is calculated for $\mathbf{r} \in V^{\text{mod}}$ as a sum of $\mathbf{E}^{s,A}$ and $\mathbf{E}^{0,A}$ from steps 3 and 7;
(9) $\mathbf{E}(\mathbf{r})$ is calculated for $\mathbf{r} \in V^{\text{mod}}$ as a sum of $\mathbf{E}^{s}$ and $\mathbf{E}^{0}$ from steps 3 and 7 of IE-C solution;
(10) misfit gradient is calculated using eq. (34) with $\mathbf{E}^{A}$ and $\mathbf{E}$ from steps 8 and 9.

In the following we refer to this scheme as the 'IE-G' solution.

3.2 Numerical verification of the adjoint approach

To verify calculation of the misfit gradient using the adjoint approach we consider a 3-D model which consists of a deep-seated non-uniform layer located between 500 and 600 km depth. The conductivity distribution in the layer (in logarithmic scale) is shown in the upper left-hand plot of Fig. 5. The anomaly has a conductivity of 1 S m^{-1}, whereas the surrounding area has a conductivity of 0.04 S m^{-1}. Above the non-uniform layer (from top to the bottom) sits a resistive 100 km lithosphere of conductivity 0.00001 S m^{-1}, and a 400 km upper mantle of conductivity 0.01 S m^{-1}. Below the non-uniform layer the conductivity is fixed to be 2 S m^{-1}. The model is excited by a source which is described by the first zonal harmonic. The layer is discretized in 72 × 36 cells of horizontal size 5° × 5° and radial size of 100 km. We calculate C-responses on the surface of the Earth on a mesh of 5° × 5° at 25 periods from 3.9 to 109.6 d, with a geometric step of 1.14. The gradient is calculated for the model vector $\mathbf{m}$, with $\sigma_i = 0.04$ S m^{-1} for all $i (i = 1, 2, \cdots, N^{\text{inv}})$. The right-hand plot of Fig. 2 presents (in the form of global maps) the data misfit gradient calculated by the adjoint approach. The left-hand plot shows the data misfit gradient calculated by numerical differentiation

$$\frac{\partial \phi_d}{\partial m_i} \approx \frac{\phi_d(m_i + \delta m_i) - \phi_d(m_i)}{\delta m_i}, \quad i = 1, 2, \ldots, N^{\text{inv}}. \tag{43}$$

Note that in our calculations we take $\frac{\delta m_i}{m_i} = 0.01$ for all i. It is seen from the Fig. 2 that the gradients calculated by the adjoint scheme and by numerical differentiation agree remarkably well. Fig. 3 supports this conclusion in a more quantitative way. It presents the results of comparison along the profile that is depicted by a dashed line in right-hand plot of Fig. 2. Again, one can see almost perfect agreement between two approaches for calculating data misfit gradients. But numerical differentiation required $N^{\text{inv}} + 1 = 72 \times 36 + 1$ forward modellings (per frequency) whereas the adjoint procedure required only two forward modellings (per frequency).

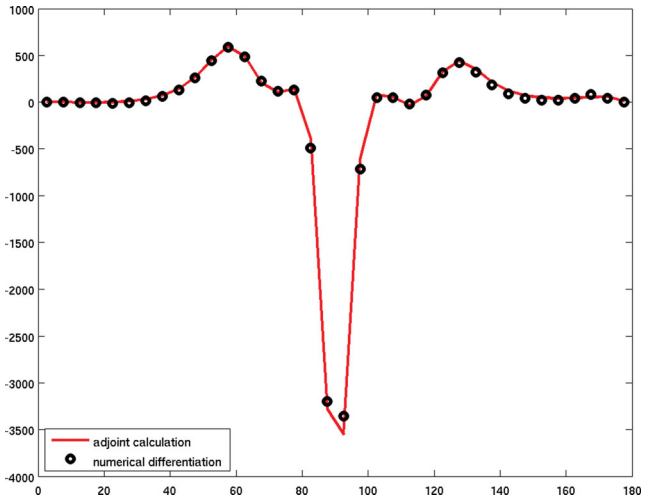

Figure 3. Comparison of the data misfit gradients along the profile depicted as a dashed line in right-hand plot of Fig. 2.

4 OPTIMIZATION AND NUMERICAL VERIFICATION OF 3-D INVERSE SOLUTION

4.1 Optimization of the inverse solution

Massive 3-D forward calculations of the responses (*cf.* IE-C scheme of Section 2.3) and misfit gradients (*cf.* IE-G scheme of Section 3.1) during the 3-D inversion dictate that these calculations have to be performed as fast as possible. Because our forward numerical schemes are based on IE formulation we can take advantage of the IE approach and perform the most time-consuming part of the forward calculations—calculations of Green's tensors, G^{ej}_{1D} (G^{ej}_{1D} is the same in IE-C and IE-G schemes), G^{hj}_{1D} (needed in IE-C scheme) and G^{eh}_{1D} (needed in IE-G scheme) only once, prior to the inversion loop. The reason for this is that Green's tensors do not depend on the 3-D conductivity distribution in the model but only on a 1-D reference conductivity distribution, which remains the same during 3-D inversion. To illustrate the gain in efficiency by using this separation scheme we provide below the CPU times (on a single processor of the ETH cluster Brutus) for major (in a sense of time consumption) components of IE forward solution at a specific frequency for a 3-D conductivity model discretized by $N_r \times N_\vartheta \times N_\varphi = 6 \times 36 \times 72 = 15552$ cells.

(i) Calculation of $G^{ej}_{1D}(\mathbf{r}, \mathbf{r}')$ for $\mathbf{r}, \mathbf{r}' \in V_{\rm mod}$ takes 270 s.
(ii) Numerical solution of scattering equation takes 30 s.
(iii) Calculation of $G^{hj}_{1D}(\mathbf{r}_a, \mathbf{r}')$ for $\mathbf{r}_a \in$ Sites and $\mathbf{r}' \in V_{\rm mod}$ takes 50 s.
(iv) Calculation of $G^{eh}_{1D}(\mathbf{r}, \mathbf{r}_a)$ for $\mathbf{r} \in V_{\rm mod}$ and $\mathbf{r}_a \in$ Sites takes 50 s.

These estimates show that separating the calculation of Green's tensors gives more than one order of magnitude acceleration (in this particular case $370/30 = 12.3$ times acceleration) of the forward calculations during inversion.

Another substantial saving of computational loads comes from parallelization of IE solution. Because forward calculations are independent with respect to frequencies we perform the modellings at $N_{\rm freq}$ frequencies in parallel on $N_{\rm freq}$ processors. This results in an additional acceleration of the forward/inversion solutions by the factor of $N_{\rm freq}$.

4.2 Numerical verification of the inverse solution

To test our inverse scheme we considered the same data, model and excitation as in Section 3.2. Our aim is to recover from the input data the conductivity distribution within the deep-seated inhomogeneous layer. The vector of parameters to be determined, $\mathbf{m}$, is the vector of logarithms of unknown electrical conductivities in $N^{\rm inv} = 72 \times 36$ cells (of 100 km thickness) comprising the inhomogeneous layer. For this test we assume known: (1) the background 1-D conductivity; (2) the geometry of the source; and (3) the location (depth and thickness) of the deep-seated inhomogeneous layer. No noise is added to the data, and no regularization is applied. Thus, this test is considered as a proof of concept, that is, we verify whether our implementation of the LMQN method along with the adjoint approach, and an optimization of the inverse solution discussed in Section 4.1 works correctly. We start the inversion using a homogeneous layer of conductivity 0.2 S m^{-1} which is far away from both the conductivity of anomaly (1 S m^{-1}) and background conductivity (0.04 S m^{-1}).

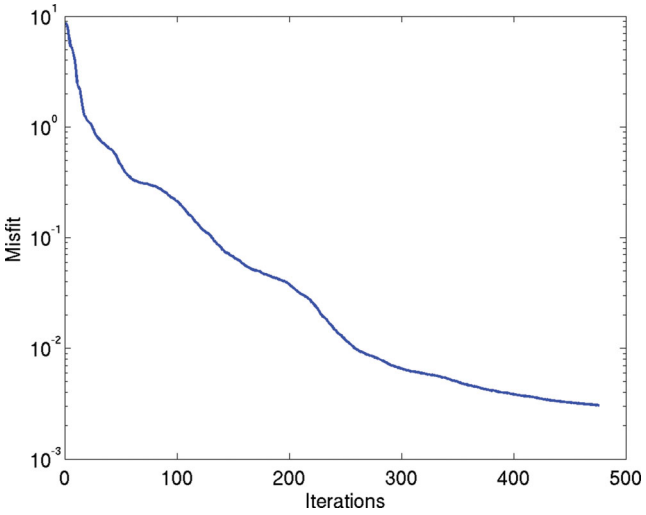

Figure 4. Normalized data misfit with respect to the inversion iterations.

Figs 4 and 5 summarize the results of our 3-D inversion test. Fig. 4 presents the normalized misfit with respect to the number of iterations. It is seen that within 150 iteration misfit drops from 10.058 to 0.067, and after 450 iterations—to 0.003. The upper left-hand plot of Fig. 5 shows the 'true' (which has to be recovered) conductivity distribution in the layer, while other plots show the evolution of conductivity recovery with respect to number of iterations in the inversion. It is seen that after 50 iterations the deep-seated anomaly is recovered fairly well, after which a further 400 iterations are necessary to recover properly the background conductivity. The final image (lower right-hand plot) almost perfectly agrees with the true conductivity.

5 CONCLUSIONS

A novel 3-D inversion technique for global electromagnetic studies in the frequency domain has been developed. It is based on the analysis of local *C*-responses and exploits a limited-memory quasi-Newton optimization method. As with most other types of optimization methods, this method requires multiple calculations of the gradient of the data misfit with respect to model parameters. We implemented the adjoint method to allow efficient calculation of the gradient.

The efficiency of 3-D inversions depends critically on the ability to perform fast forward problem calculations. Because our forward solver is based on IE formulation, we take the advantage of this approach and conduct the most time-consuming part of the simulations—calculation of the tensor Green's functions—only once, prior to the inversion. Modelling experiments performed here demonstrated that separating the calculation of Green's tensors accelerates the inverse solution by more than one order of magnitude.

Further improvement in computational time stems from the parallelization of the forward IE solver. Because forward calculations are independent with respect to frequencies, they are performed at different frequencies in parallel on N_f processors, where N_f is the number of analysed periods.

We verified our 3-D inversion scheme with synthetic data. The companion paper by Semenov & Kuvshinov (2012) reports an application of our 3-D inverse solution to real data—a set of local *C*-responses estimated at a global net of geomagnetic observatories.

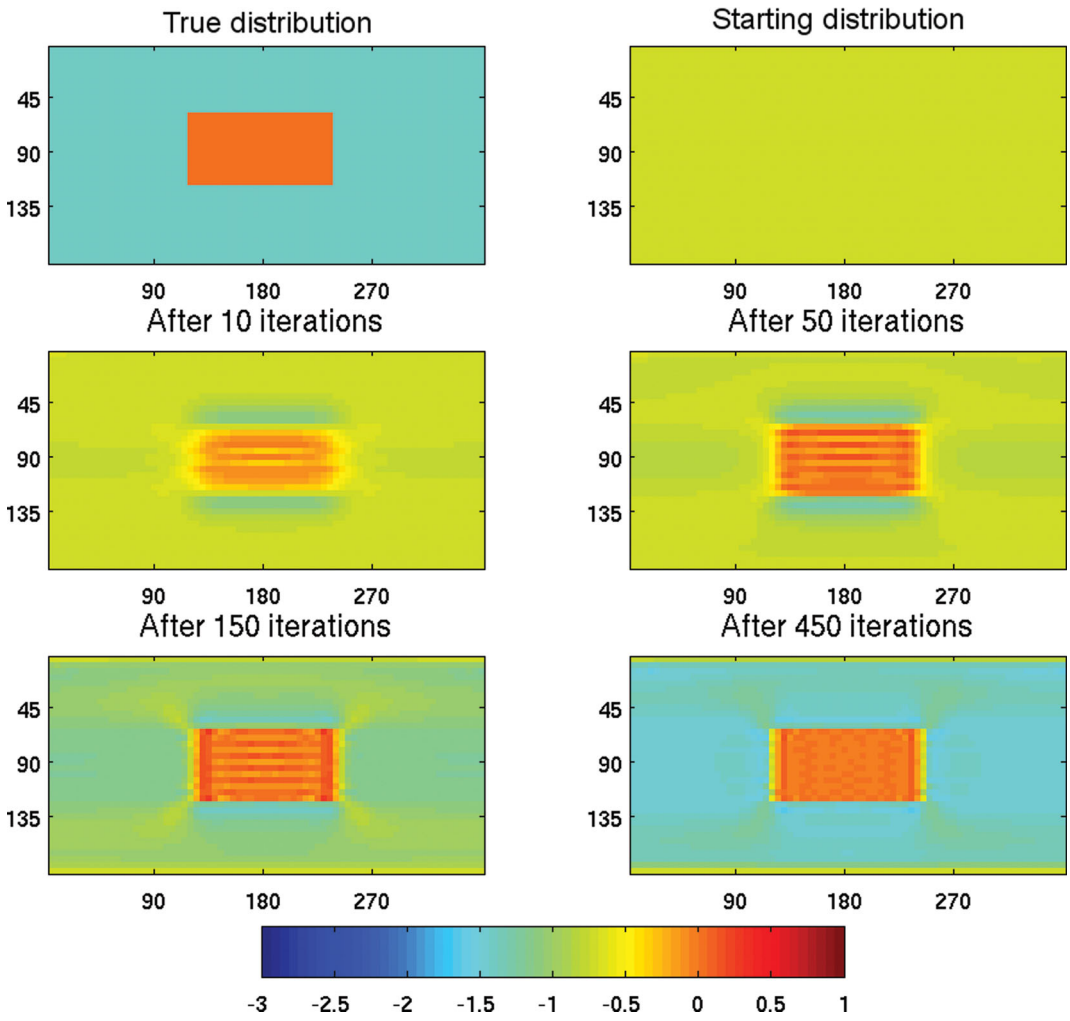

Figure 5. True conductivity distribution (upper left-hand plot) and the results of conductivity recovery with respect to inversion iteration. The results are presented in logarithmic scale.

ACKNOWLEDGMENTS

The authors thank Amir Khan and Chris Finlay for help with improving the presentation of this paper. This work has been supported by ETH grant No. 0-20423-07, and in part by European Space Agency through ESTEC contracts No. 20944/07/NL/JA and No. 22656/09/NL/FF, and by the Russian Foundation for Basic Research under grant No. 09-05-01071-a.

REFERENCES

Avdeev, D.B. & Avdeeva, A., 2009. 3-D magnetotelluric inversion using a limited-memory quasi-Newton optimization, *Geophysics,* **74,** 45–57.

Backus, G., Parker, R.L. & Constable, C.G., 1996. *Foundations of Geomagnetism,* Cambridge University Press, Cambridge.

Banks, R., 1969. Geomagnetic variations and the electrical conductivity of the upper mantle, *Geophys. J. R. astr. Soc.,* **17,** 457–487.

Fainberg, E., Kuvshinov, A. & Singer, B., 1990. Electromagnetic induction in a spherical Earth with non-uniform oceans and continents in electric contact with the underlying medium—I. Theory, method, example, *Geophys. J. Int.,* **102,** 273–281.

Fujii, I. & Schultz, A., 2002. The 3D electromagnetic response of the Earth to the ring current and auroral oval excitation, *Geophys. J. Int.,* **151,** 689–709.

Fukao, Y., Koyama, T., Obayashi, M. & Utada, H., 2004. Trans-Pacific temperature field in the mantle transition region derived from seismic and electromagnetic tomography, *Earth planet Sci. Lett.,* **211,** 425–434.

Haber, E., 2005. Quasi-Newton methods for large-scale electromagnetic inverse problems, *Inverse Probl.,* **21,** 305–323.

Jackson, J., 1975. *Classical Electrodynamics,* John Wiley & Sons, New York, NY.

Kelbert, A., Egbert, G. & Schultz, A., 2008. A nonlinear conjugate 3-D inversion of global induction data. Resolution studies, *Geophys. J. Int.,* **173,** 365–381.

Kelbert, A., Schultz, A. & Egbert, G., 2009. Global electromagnetic induction constraints on transition-zone water content variations, *Nature,* **460,** 1003–1007.

Khan, A., Boschi, L. & Connolly, J., 2009. On mantle chemical and thermal heterogeneities and anisotropy as mapped by inversion of global surface wave data, *J. geophys. Res.,* **111,** B10102 doi:10.1029/2006JB004270.

Koyama, T., 2001. A study on the electrical conductivity of the mantle by voltage measurements of submarine cables, *PhD thesis*, University of Tokyo, Japan.

Koyama, T., Shimizu, H., Utada, H., Ichiki, M., Ohtani, E. & Hae, R., 2006. Water content in the mantle transition zone beneath the North Pacific derived from the electrical conductivity anomaly, *Am. geophys. Un. Monogr. Ser.,* **168,** 171–179.

Kustowski, B., Ekström, G. & Dziewoński, A.M., 2008. Anisotropic shear-wave velocity structure of the Earth's mantle: a global model, *J. geophys. Res.,* **113,** doi:10.1029/2007JB005169.

Kuvshinov, A., 2008. 3-D global induction in the oceans and solid Earth: recent progress in modeling magnetic and electric fields from sources of magnetospheric, ionospheric and oceanic origin, *Surv. Geophys.,* **29,** doi:10.1007/s10712-008-9045-z.

Kuvshinov, A.V., Avdeev, D.B., Pankratov, O.V., Golyshev, S.A. & Olsen, N., 2002. Modelling electromagnetic fields in 3D spherical Earth using fast integral equation approach, in *3D Electromagnetics,* ch. 3, pp. 43–54, eds Zhdanov, M.S. & Wannamaker, P.E., Elsevier, Amsterdam.

Newman, G. & Alumbaugh, D.L., 2000. Three-dimensional magnetotelluric inversion using non-linear conjugate gradients, *Geophys. J. Int.,* **140,** 410–424.

Nocedal, J. & Wright, S.J., 2006. *Numerical Optimization,* Springer, New York, NY.

Pankratov, O. & Kuvshinov, A., 2010a. General formalism for the efficient calculation of derivatives of EM frequency domain responses and derivatives of the misfit, *Geophys. J. Int.,* **181,** 229–249.

Pankratov, O. & Kuvshinov, A., 2010b. Fast calculation of the sensitivity matrix for responses to the Earth's conductivity: general strategy and examples, *Phys. Solid Earth,* **46,** 788–804.

Pankratov, O., Avdeyev, D. & Kuvshinov, A., 1995. Electromagnetic field scattering in a heterogeneous Earth: a solution to the forward problem, *Phys. Solid Earth,* **31,** 201–209.

Panning, M. & Romanovicz, B., 2006. A three-dimensional radially anisotropic model of shear velocity in the whole mantle, *Geophys. J. Int.,* **167,** 361–379, doi:10.1111/j.1365-246X.2006.03100.x.

Plessix, R.-E. & Mulder, M., 2008. Resistivity imaging with controlled source electromagnetic data: depth and data weighting, *Inverse Probl.,* **24,** 1–22.

Roberts, R.G., 1984. The long-period electromagnetic response of the Earth, *Geophys. J. R. astr. Soc.,* **78,** 547–572.

Rodi, W. & Mackie, R.L., 2000. Nonlinear conjugate gradients algorithm for 2-D magnetotelluric inversion, *Geophysics,* **66,** 174–187.

Rokityansky, I., 1982. *Geoelectromagnetic Investigation of the Earth's Crust and Mantle,* Springer, Berlin.

Schultz, A.J., 1987. On the electrical conductivity of the mid-mantle—I. calculation of equivalent scalar magnetotelluric response functions, *Geophys. J. Int.,* **88**(3), 733–761.

Semenov, A. & Kuvshinov, A., 2012. Global 3-D imaging of mantle conductivity based on inversion of observatory *C*-responses—II. Data analysis and results, *Geophys. J. Int,* submitted.

Shimizu, H., Utada, H., Baba, K., Koyama, T., Obayashi, M. & Fukao, Y., 2010. Three-dimensional imaging of electrical conductivity in the mantle transition zone beneath the North Pacific Ocean by a semi-global induction study, *Phys. Earth planet Int.,* **183,** doi:10.1016/j.pepi.

Singer, B., 1995. Method for solution of Maxwell's equations in non-uniform media, *Geophys. J. Int.,* **120,** 590–598.

Singer, B., 2008. Electromagnetic integral equation approach based on contraction operator and solution optimization in Krylov subspace, *Geophys. J. Int.,* **175,** 857–884.

Tarits, P. & Mandea, M., 2010. The heterogeneous electrical conductivity structure of the lower mantle, *Phys. Earth planet. Int.,* **183,** doi:10.1016/j.pepi.2010.08.002.

Trampert, J., Deschamps, F., Resovsky, J. & Yuen, D., 2004. Chemical heterogeneities throughout the lower mantle, *Science,* **306,** 853–855.

Utada, H., Koyama, T., Obayashi, M. & Fukao, Y., 2009. A joint interpretation of electromagnetic and seismic tomography models suggests the mantle transition zone below Europe is dry, *Earth planet. Sci. Lett.,* **281,** 249–257.

Weidelt, P., 1972. The inverse problem of geomagnetic induction, *Z. Geophys.,* **38,** 257–289.

APPENDIX A: HELMHOLTZ REPRESENTATION

In this Appendix, we introduce Helmholtz representation (on a sphere) of a general vector field; this respresentation will be used in Appendix B. Consider vector field **F**. Then the equation

$$\mathbf{F} = U\mathbf{e}_r + \nabla_\perp V + \mathbf{e}_r \times \nabla_\perp W, \tag{A1}$$

defines the Helmholtz representation of **F** in terms of a radial vector field $U\mathbf{e}_r$ and horizontal vector field $\nabla_\perp V + \mathbf{e}_r \times \nabla_\perp W$. Here $\nabla_\perp$ is the angular part of operator $\nabla = \mathbf{e}_r \frac{\partial}{\partial r} + \frac{1}{r}\nabla_\perp$, $\mathbf{e}_r$ is the outward unit vector, and '$\times$' denotes a vector (cross) product. This representation can be shown to be unique (*cf.* Backus *et al.* 1996) if for any value r within a shell, the average values of V and W over the sphere of radius r (denoted as $\langle\rangle_{S(r)}$) is such that

$$\langle V\rangle_{S(r)} = \langle W\rangle_{S(r)} = 0. \tag{A2}$$

Each of scalar function U, V, W can be expanded in terms of spherical harmonics in the form

$$U(r,\theta,\varphi) = \sum_{n=0}^{\infty}\sum_{m=-n}^{n} U_{mn}(r) S_n^m(\theta,\varphi), \tag{A3}$$

where $S_n^m(\vartheta,\varphi) = P_n^{|m|}(\cos\vartheta)e^{im\varphi}$, $P_n^{|m|}$ are the associated Legendre polynomials of degree n ($n = 0, 1, \ldots$) and of order $|m|$. Note that for V and W the $n = 0$ term is zero because of eq. (A2). Substituting eq. (A3) and similar expansions for V and W into eq. (A1) we obtain

$$\mathbf{F}(r,\theta,\varphi) = \sum_{n=0}^{\infty}\sum_{m=-n}^{n} U_{mn}(r) S_n^m(\theta,\varphi)\mathbf{e}_r + \sum_{n=1}^{\infty}\sum_{m=-n}^{n} V_{mn}(r)\nabla_\perp S_n^m(\theta,\varphi) + \sum_{n=1}^{\infty}\sum_{m=-n}^{n} W_{mn}(r)\mathbf{e}_r \times \nabla_\perp S_n^m(\theta,\varphi). \tag{A4}$$

Note that if **F** stands for the magnetic field or electric current then the terms for $n = 0$, in corresponding radial components, are also zero, because the magnetic field and electric current are solenoidal vector fields (*cf.* Backus *et al.* 1996).

APPENDIX B: DERIVATION OF GREEN'S TENSORS G^{ej}_{1D} AND G^{hj}_{1D}

In this Appendix, we derive the explicit forms of a 3×3 tensor 'current-to-electric' and 'current-to-magnetic' Green's functions for an Earth model with a radially symmetric distributed electrical conductivity $\sigma_0(r)$. These Green's tensors allow the calculation of magnetic and electric

fields that obey Maxwell's equations

$$\nabla \times \mathbf{H} = \sigma_0(r)\mathbf{E} + \mathbf{j}, \tag{B1}$$

$$\nabla \times \mathbf{E} = \mathrm{i}\omega\mu_0\mathbf{H}, \tag{B2}$$

in the following integral form

$$\mathbf{E}(r, \vartheta, \varphi) = \int_V G^{ej}_{1\mathrm{D}}(r, r', \vartheta, \vartheta', \varphi - \varphi')\mathbf{j}(r', \vartheta', \varphi')\,\mathrm{d}v', \tag{B3}$$

$$\mathbf{H}(r, \vartheta, \varphi) = \int_V G^{hj}_{1\mathrm{D}}(r, r', \vartheta, \vartheta', \varphi - \varphi')\mathbf{j}(r', \vartheta', \varphi')\,\mathrm{d}v'. \tag{B4}$$

Here, V is a 3-D volume occupied by a current $\mathbf{j}$, $\mathrm{d}v' = r'^2 \sin\vartheta' \mathrm{d}r' \mathrm{d}\vartheta' \mathrm{d}\varphi'$ and

$$G^{ej(hj)}_{1\mathrm{D}} = \mathbf{e}_\vartheta g^{ej(hj)}_{\vartheta\vartheta'}\mathbf{e}_{\vartheta'} + \mathbf{e}_\vartheta g^{ej(hj)}_{\vartheta\varphi'}\mathbf{e}_{\varphi'} + \cdots + \mathbf{e}_r g^{ej(hj)}_{rr'}\mathbf{e}_{r'}, \tag{B5}$$

where $\mathbf{e}_r$, $\mathbf{e}_\vartheta$, $\mathbf{e}_\varphi$ and $\mathbf{e}_{r'}$, $\mathbf{e}_{\vartheta'}$, $\mathbf{e}_{\varphi'}$ are the unit vectors of spherical coordinate system at points $\mathbf{r} = (r, \vartheta, \varphi)$ and $\mathbf{r}' = (r', \vartheta', \varphi')$, respectively. Note that Kuvshinov *et al.* (2002) (see also Kuvshinov 2008) presented expressions for elements $g^{ej(hj)}_{\vartheta\vartheta'}, g^{ej(hj)}_{\vartheta\varphi'}, \ldots, g^{ej(hj)}_{rr'}$ but without details of how these expressions have been derived. Here, and in the following Appendices C–F we provide the omitted details.

First, we consider the spherical vector functions, which are determined via the spherical scalar function $S^n_m(\vartheta, \varphi)$ as

$$\mathbf{S}^r_{nm}(\vartheta, \varphi) = S^n_m(\vartheta, \varphi)\mathbf{e}_r, \tag{B6}$$

$$\mathbf{S}^t_{nm}(\vartheta, \varphi) = \frac{1}{\sqrt{n(n+1)}}\mathbf{e}_r \times \nabla_\perp S^m_n(\vartheta, \varphi), \tag{B7}$$

$$\mathbf{S}^p_{nm}(\vartheta, \varphi) = \frac{1}{\sqrt{n(n+1)}}\nabla_\perp S^m_n(\vartheta, \varphi). \tag{B8}$$

The coefficient $\frac{1}{\sqrt{n(n+1)}}$ is introduced to ensure that $\mathbf{S}^t_{nm}$ and $\mathbf{S}^p_{nm}$ have the same norm as $\mathbf{S}^r_{nm}$. Following the Helmholtz representation as discussed in Appendix A, the horizontal and radial components of the electric field, $\mathbf{E}$, and electric current, $\mathbf{j}$, can be decomposed as follows

$$\mathbf{E}_\tau(r, \vartheta, \varphi) = \frac{1}{r}\sum_{n,m}\left\{\varepsilon^t_{nm}(r)\mathbf{S}^t_{nm}(\vartheta, \varphi) + \varepsilon^p_{nm}(r)\mathbf{S}^p_{nm}(\vartheta, \varphi)\right\}, \tag{B9}$$

$$E_r(r, \vartheta, \varphi)\mathbf{e}_r = \frac{1}{r}\sum_{n,m}\varepsilon^r_{nm}(r)\mathbf{S}^r_{nm}, \tag{B10}$$

$$\mathbf{j}_\tau(r, \vartheta, \varphi) = \frac{1}{r}\sum_{n,m}\left\{j^t_{nm}(r)\mathbf{S}^t_{nm}(\vartheta, \varphi) + j^p_{nm}(r)\mathbf{S}^p_{nm}(\vartheta, \varphi)\right\}, \tag{B11}$$

$$j_r(r, \vartheta, \varphi)\mathbf{e}_r = \frac{1}{r}\sum_{n,m}j^r_{nm}(r)\mathbf{S}^r_{nm}. \tag{B12}$$

Hereinafter $\sum_{n,m}$ denotes the summation $\sum_{n=1}^{\infty}\sum_{m=-n}^{n}$. Note that for the radial part of the electric field the term for $n = 0$ is also equal to zero, as is clear from eq. (B17). Factor $\frac{1}{r}$ is introduced to simplify the forthcoming calculations. For the magnetic field we have a similar decomposition but we write the horizontal part of the field in a slightly different manner,

$$\mathbf{e}_r \times \mathbf{H}_\tau(r, \vartheta, \varphi) = \frac{1}{r}\sum_{n,m}\left\{h^t_{nm}(r)\mathbf{S}^t_{nm}(\vartheta, \varphi) + h^p_{nm}(r)\mathbf{S}^p_{nm}(\vartheta, \varphi)\right\}, \tag{B13}$$

leaving a similar (as for the electric field and impressed current) decomposition of the radial part

$$H_r(r, \vartheta, \varphi)\mathbf{e}_r = \frac{1}{r}\sum_{n,m}h^r_{nm}(r)\mathbf{S}^r_{nm}(\vartheta, \varphi). \tag{B14}$$

Substituting eqs (B9)–(B14) into eqs (B1)–(B2) and gathering terms involving the functions $\mathbf{S}^t_{nm}$ and $\mathbf{S}^p_{nm}$, we derive the system of equations

$$\begin{cases}\partial_r\varepsilon^t_{nm} = -\mathrm{i}\omega\mu_0 h^t_{nm},\\ \partial_r h^t_{nm} = -\frac{\kappa^2}{\mathrm{i}\omega\mu_0}\varepsilon^t_{nm} + j^t_{nm},\end{cases} \tag{B15}$$

to determine the coefficients ε^t_{nm} and h^t_{nm}, and the system

$$\begin{cases}\partial_r\varepsilon^p_{nm} = \frac{\kappa^2}{\sigma_0}h^p_{nm} - \frac{\sqrt{n(n+1)}}{r\sigma_0}j^r_{nm},\\ \partial_r h^p_{nm} = \sigma_0\varepsilon^p_{nm} + j^p_{nm},\end{cases} \tag{B16}$$

to determine the coefficients ε^p_{nm} and h^p_{nm}. Here $\kappa^2 = \frac{n(n+1)}{r^2} - \mathrm{i}\omega\mu_0\sigma_0$. For determination of the coefficients ε^r_{nm} and h^r_{nm} we derive the following equations

$$\sigma_0\varepsilon^r_{nm} = \frac{\sqrt{n(n+1)}}{r}h^p_{nm} - j^r_{nm}, \tag{B17}$$

$$\mathrm{i}\omega\mu_0 h^r_{nm} = -\frac{\sqrt{n(n+1)}}{r}\varepsilon^t_{nm}. \tag{B18}$$

The systems of eqs (B15) and (B16) can be written in the following generic form

$$\begin{cases} \partial_r\varepsilon(r) = p(r)h(r) + f_h(r), \\ \partial_r h(r) = q\varepsilon(r) + f_\varepsilon(r), \end{cases} \tag{B19}$$

where

$$\begin{aligned} &\varepsilon(r) = \varepsilon^t_{nm}, \qquad h(r) = h^t_{nm}, \\ &p(r) = -\mathrm{i}\omega\mu_0, \qquad q(r) = -\frac{\kappa^2}{\mathrm{i}\omega\mu_0}, \\ &f_\varepsilon(r) = j^t_{nm}, \qquad f_h(r) = 0, \end{aligned} \tag{B20}$$

for system (B15) and

$$\begin{aligned} &\varepsilon(r) = \varepsilon^p_{nm}, \qquad h(r) = h^p_{nm}, \\ &p(r) = \frac{\kappa^2}{\sigma_0}, \qquad q(r) = \sigma_0, \\ &f_\varepsilon(r) = j^p_{nm}, \qquad f_h(r) = -\frac{\sqrt{n(n+1)}}{r\sigma_0}j^r_{nm}, \end{aligned} \tag{B21}$$

for system (B16). System (B19) can be reduced to the second order ordinary differential equation

$$\partial_r\left[\frac{1}{p(r)}\partial_r\varepsilon(r)\right] - q(r)\varepsilon(r) = f(r), \tag{B22}$$

where

$$f(r) = f_\varepsilon(r) + \partial_r\left[\frac{f_h(r)}{p(r)}\right]. \tag{B23}$$

The solution of eq. (B22) can be written as

$$\varepsilon(r) = \int_0^\infty G(n, r, r')f(r')\,\mathrm{d}r', \tag{B24}$$

where $G(n, r, r')$ is the scalar Green's function of eq. (B22). The explicit forms of $G(n, r, r')$ are presented in Appendix D. We impose the boundary conditions on the solution of eq. (B22) in the form $\varepsilon(r) \to 0$, when $r \to 0$ and $r \to \infty$.

Substituting eq. (B23) into eq. (B24) and integrating by parts, we have

$$\varepsilon(r) = \int_0^\infty G(n, r, r')f_\varepsilon(r')\,\mathrm{d}r' - \int_0^\infty \beta(n, r, r')G(n, r, r')f_h(r')\,\mathrm{d}r', \tag{B25}$$

where we define β as

$$\beta(n, r, r') = \frac{\partial_{r'}G(n, r, r')}{p(r')G(n, r, r')}. \tag{B26}$$

Then, substituting eq. (B25) into the first equation of the system (B19), we obtain in a similar fashion

$$h(r) = \int \alpha(n, r, r')G(n, r, r')f_\varepsilon(r')\,\mathrm{d}r' - \int \alpha(n, r, r')\beta(n, r, r')G(n, r, r')f_h(r')\,\mathrm{d}r', \tag{B27}$$

where we denote

$$\alpha(n, r, r') = \beta(n, r', r). \tag{B28}$$

An explicit formula for $\alpha(n, r, r')$ is presented in Appendix D. Note that while deriving eq. (B27) we used the relation

$$\partial_r\beta(n, r, r') = -\frac{\delta(r - r')}{G(n, r, r)}. \tag{B29}$$

Substituting eqs (B20) and (B21) into eqs (B25) and (B27) we express coefficients ε^t_{nm}, ε^p_{nm}, h^t_{nm} and h^p_{nm} via the coefficients j^t_{nm}, j^p_{nm} and j^r_{nm} as

$$\varepsilon^t_{nm}(r) = \int_0^\infty G^t(n, r, r')j^t_{nm}(r')\,\mathrm{d}r', \tag{B30}$$

$$\varepsilon^p_{nm}(r) = \int_0^\infty G^p(n,r,r')j^p_{nm}(r')\,\mathrm{d}r' + \int_0^\infty \frac{\sqrt{n(n+1)}}{r'\sigma_0(r')}\beta^p(n,r,r')G^p(n,r,r')j^r_{nm}(r')\,\mathrm{d}r', \tag{B31}$$

$$h^t_{nm}(r) = \int_0^\infty \alpha^t(n,r,r')G^t(n,r,r')j^t_{nm}(r')\,\mathrm{d}r', \tag{B32}$$

$$h^p_{nm}(r) = \int_0^\infty \alpha^p(n,r,r')G^p(n,r,r')j^p_{nm}(r')\,\mathrm{d}r' + \\ + \int_0^\infty \frac{\sqrt{n(n+1)}}{r'\sigma_0(r')}\alpha^p(n,r,r')\beta^p(n,r,r')G^p(n,r,r')j^r_{nm}(r')\,\mathrm{d}r'. \tag{B33}$$

Then, using decompositions (B11) and (B12), the coefficients j^t_{nm}, j^p_{nm} and j^r_{nm} are written as

$$j^t_{nm}(r) = \frac{r}{\|S^m_n\|^2\sqrt{n(n+1)}}\int_\Omega \nabla'_\perp\cdot(\mathbf{e}_{r'}\times\mathbf{j}_\tau)\widetilde{S^m_n}\mathrm{d}\Omega', \tag{B34}$$

$$j^p_{nm}(r) = -\frac{r}{\|S^m_n\|^2\sqrt{n(n+1)}}\int_\Omega (\nabla'_\perp\cdot\mathbf{j}_\tau)\widetilde{S^m_n}\mathrm{d}\Omega', \tag{B35}$$

$$j^r_{nm}(r) = \frac{r}{\|S^m_n\|^2}\int_\Omega j_r\widetilde{S^m_n}\mathrm{d}\Omega'. \tag{B36}$$

Here Ω is the complete solid angle and $\mathrm{d}\Omega' = \sin\vartheta'\mathrm{d}\vartheta'\mathrm{d}\varphi'$. $\widetilde{S^m_n}$ stands for the complex conjugate of S^m_n, and $\|S^m_n\|^2$ denotes the squared norm of S^m_n. When deriving eqs (B34) and (B35) we used the facts that

$$\nabla_\perp\cdot(\mathbf{e}_r\times\nabla_\perp) = 0, \tag{B37}$$

$$\Delta_\perp S^m_n = -n(n+1)S^m_n. \tag{B38}$$

Here operators $\nabla_\perp\cdot$ and $\Delta_\perp$ stand for the angular parts of the divergence and the Laplacian, respectively. More explicitly, the action of these operators on any entry functions $\mathbf{a}_\tau = a_\vartheta\mathbf{e}_\vartheta + a_\varphi\mathbf{e}_\varphi$ and u is defined as

$$\nabla_\perp\cdot\mathbf{a}_\tau = \frac{1}{\sin\vartheta}\frac{\partial(a_\vartheta\sin\vartheta)}{\partial\vartheta} + \frac{1}{\sin\vartheta}\frac{\partial a_\varphi}{\partial\varphi}, \tag{B39}$$

$$\Delta_\perp u = \nabla_\perp\cdot(\nabla_\perp u) = \frac{1}{\sin\vartheta}\frac{\partial}{\partial\vartheta}\left(\sin\vartheta\frac{\partial u}{\partial\vartheta}\right) + \frac{1}{\sin^2\vartheta}\frac{\partial^2 u}{\partial\varphi^2}. \tag{B40}$$

Substituting eqs (B34)–(B36) into eqs (B30)–(B31) and further eqs (B30)–(B31) into eq. (B9) we obtain for the horizontal part of the electric field, after rearranging the operations of integration and summation

$$\begin{aligned}\mathbf{E}_\tau(r,\vartheta,\varphi) = &\int_\Omega\int_0^\infty(\mathbf{e}_r\times\nabla_\perp)\left\{\left[(\mathbf{e}_{r'}\times\nabla'_\perp)\mathcal{P}\left[\frac{r'}{r}\frac{G^t(n,r,r')}{n(n+1)}\right]\right]\cdot\mathbf{j}_\tau(r',\vartheta',\varphi')\right\}\mathrm{d}r'\mathrm{d}\Omega' \\ &+\int_\Omega\int_0^\infty\nabla_\perp\left\{\left[\nabla'_\perp\mathcal{P}\left[\frac{r'}{r}\frac{G^p(n,r,r')}{n(n+1)}\right]\right]\cdot\mathbf{j}_\tau(r',\vartheta',\varphi')\right\}\mathrm{d}r'\mathrm{d}\Omega' \\ &-\int_\Omega\int_0^\infty\nabla_\perp\left\{\mathcal{P}\left[\frac{\beta^p(n,r,r')G^p(n,r,r')}{r\sigma_0(r')}\right]j_r(r',\vartheta',\varphi')\right\}\mathrm{d}r'\mathrm{d}\Omega'.\end{aligned} \tag{B41}$$

Here '$\cdot$' stands for the scalar product of two vectors, and $\mathcal{P}[f]$ denotes the summation of series

$$\mathcal{P}\big[f(n,r,r')\big] = \sum_{n=1}^\infty\frac{2n+1}{4\pi}f(n,r,r')P_n(\cos\gamma), \tag{B42}$$

where P_n are the Legendre polynomials, and $\cos\gamma$ is determined by

$$\cos\gamma = \cos\vartheta\cos\vartheta' + \sin\vartheta\sin\vartheta'\cos(\varphi-\varphi'). \tag{B43}$$

Note that while deriving eq. (B41) we used the theorem of summation for spherical functions (*cf.* Jackson 1975)

$$\sum_{n=0}^\infty\sum_{m=-n}^n\frac{S^m_n(\vartheta,\varphi)\widetilde{S^m_n}(\vartheta',\varphi')}{\|S^m_n\|^2} = \sum_{n=0}^\infty\frac{2n+1}{4\pi}P_n(\cos\gamma), \tag{B44}$$

and the following equalities

$$\int_\Omega Q\nabla'_\perp\cdot\mathbf{P}\,\mathrm{d}\Omega' = -\int_\Omega\mathbf{P}\nabla'_\perp Q\,\mathrm{d}\Omega', \tag{B45}$$

$$\mathbf{a}(\mathbf{b}\times\mathbf{c}) = -(\mathbf{b}\times\mathbf{a})\mathbf{c}, \tag{B46}$$

that are valid for any scalar function Q and any vector functions $\mathbf{P}$, $\mathbf{a}$, $\mathbf{b}$ and $\mathbf{c}$. In a similar way we obtain the expressions for the radial component of the electric field

$$\begin{aligned} E_r(r,\vartheta,\varphi) = &-\frac{1}{\sigma_0(r)} j_r(r,\vartheta,\varphi) \\ &- \int_\Omega\int_0^\infty \left[\Delta'_\perp \mathcal{P}\left[\frac{\alpha^p(n,r,r')\beta^p(n,r,r')G^p(n,r,r')}{r^2\sigma_0(r)\sigma_0(r')}\right]\right] j_r(r',\vartheta',\varphi')\,\mathrm{d}r'\mathrm{d}\Omega' \\ &+ \int_\Omega\int_0^\infty \left[\nabla'_\perp \mathcal{P}\left[\frac{r'}{r^2}\alpha^p(n,r,r')G^p(n,r,r')\right]\right]\cdot\mathbf{j}_\tau(r',\vartheta',\varphi')\,\mathrm{d}r'\mathrm{d}\Omega', \end{aligned} \tag{B47}$$

and for the horizontal and radial components of the magnetic field

$$\begin{aligned} \mathbf{H}_\tau(r,\vartheta,\varphi) = &\int_\Omega\int_0^\infty \nabla_\perp \left\{\left[(\mathbf{e}_{r'}\times\nabla'_\perp)\mathcal{P}\left[\frac{r'}{r}\frac{\alpha^t(n,r,r')G^t(n,r,r')}{n(n+1)}\right]\right]\cdot\mathbf{j}_\tau(r',\vartheta',\varphi')\right\}\mathrm{d}r'\mathrm{d}\Omega' \\ &- \int_\Omega\int_0^\infty (\mathbf{e}_r\times\nabla_\perp)\left\{\left[\nabla'_\perp\mathcal{P}\left[\frac{r'}{r}\frac{\alpha^p(n,r,r')G^p(n,r,r')}{n(n+1)}\right]\right]\cdot\mathbf{j}_\tau(r',\vartheta',\varphi')\right\}\mathrm{d}r'\mathrm{d}\Omega' \\ &- \int_\Omega\int_0^\infty (\mathbf{e}_r\times\nabla_\perp)\left\{\mathcal{P}\left[\frac{\alpha^p(n,r,r')\beta^p(n,r,r')G^p(n,r,r')}{r\sigma_0(r')}\right] j_r(r',\vartheta',\varphi')\right\}\mathrm{d}r'\mathrm{d}\Omega', \end{aligned} \tag{B48}$$

$$H_r(r,\vartheta,\varphi) = -\int_\Omega\int_0^\infty \left[(\mathbf{e}_{r'}\times\nabla'_\perp)\mathcal{P}\left[\frac{r'}{r^2}\frac{G^p(n,r,r')}{i\omega\mu_0}\right]\right]\cdot\mathbf{j}_\tau(r',\vartheta',\varphi')\,\mathrm{d}r'\mathrm{d}\Omega'. \tag{B49}$$

Now from eqs (B41) and (B47) we write the expressions for elements $g^{ej}_{\vartheta\vartheta'}, g^{ej}_{\vartheta\varphi'}, \ldots, g^{ej}_{rr'}$ of eq. (B5)

$$g^{ej}_{\vartheta\vartheta'} = \frac{1}{\sin\vartheta}\frac{1}{\sin\vartheta'}\partial_\varphi\partial_{\varphi'}\mathcal{P}\left[\frac{1}{r'r}\frac{G^t}{n(n+1)}\right] + \partial_\vartheta\partial_{\vartheta'}\mathcal{P}\left[\frac{1}{r'r}\frac{G^p}{n(n+1)}\right], \tag{B50}$$

$$g^{ej}_{\vartheta\varphi'} = -\frac{1}{\sin\vartheta}\partial_\varphi\partial_{\vartheta'}\mathcal{P}\left[\frac{1}{r'r}\frac{G^t}{n(n+1)}\right] + \frac{1}{\sin\vartheta'}\partial_\vartheta\partial_{\varphi'}\mathcal{P}\left[\frac{1}{r'r}\frac{G^p}{n(n+1)}\right], \tag{B51}$$

$$g^{ej}_{\vartheta r'} = -\partial_\vartheta\mathcal{P}\left[\frac{1}{r'^2r}\frac{\beta^pG^p}{\sigma_0(r')}\right], \tag{B52}$$

$$g^{ej}_{\varphi\vartheta'} = -\frac{1}{\sin\vartheta'}\partial_\vartheta\partial_{\varphi'}\mathcal{P}\left[\frac{1}{r'r}\frac{G^t}{n(n+1)}\right] + \frac{1}{\sin\vartheta}\partial_\varphi\partial_{\vartheta'}\mathcal{P}\left[\frac{1}{r'r}\frac{G^p}{n(n+1)}\right], \tag{B53}$$

$$g^{ej}_{\varphi\varphi'} = \partial_\vartheta\partial_{\vartheta'}\mathcal{P}\left[\frac{1}{r'r}\frac{G^t}{n(n+1)}\right] + \frac{1}{\sin\vartheta}\frac{1}{\sin\vartheta'}\partial_\varphi\partial_{\varphi'}\mathcal{P}\left[\frac{1}{r'r}\frac{G^p}{n(n+1)}\right], \tag{B54}$$

$$g^{ej}_{\varphi r'} = -\frac{1}{\sin\vartheta}\partial_\varphi\mathcal{P}\left[\frac{1}{r'^2r}\frac{\beta^pG^p}{\sigma_0(r')}\right], \tag{B55}$$

$$g^{ej}_{r\vartheta'} = \partial_{\vartheta'}\mathcal{P}\left[\frac{1}{r'r^2}\frac{\alpha^pG^p}{\sigma_0(r)}\right], \tag{B56}$$

$$g^{ej}_{r\varphi'} = \frac{1}{\sin\vartheta'}\partial_{\varphi'}\mathcal{P}\left[\frac{1}{r'r^2}\frac{\alpha^pG^p}{\sigma_0(r)}\right], \tag{B57}$$

$$g^{ej}_{rr'} = -\frac{\delta(r-r')\delta(\vartheta-\vartheta')\delta(\varphi-\varphi')}{r'^2\sin\vartheta'\sigma_0(r)} + \mathcal{P}\left[\frac{1}{r'^2r^2}\frac{n(n+1)\alpha^p\beta^pG^p}{\sigma_0(r)\sigma_0(r')}\right]. \tag{B58}$$

In a similar way from eqs (B48) and (B49) we write the expressions for elements $g^{hj}_{\vartheta\vartheta'}, g^{hj}_{\vartheta\varphi'}, \ldots, g^{hj}_{rr'}$ of eq. (B5)

$$g^{hj}_{\vartheta\vartheta'} = -\frac{1}{\sin\vartheta'}\partial_\vartheta\partial_{\varphi'}\mathcal{P}\left[\frac{1}{r'r}\frac{\alpha^tG^t}{n(n+1)}\right] + \frac{1}{\sin\vartheta}\partial_\varphi\partial_{\vartheta'}\mathcal{P}\left[\frac{1}{r'r}\frac{\alpha^pG^p}{n(n+1)}\right], \tag{B59}$$

$$g^{hj}_{\varphi\vartheta'} = -\frac{1}{\sin\vartheta}\frac{1}{\sin\vartheta'}\partial_\varphi\partial_{\varphi'}\mathcal{P}\left[\frac{1}{r'r}\frac{\alpha^tG^t}{n(n+1)}\right] - \partial_\vartheta\partial_{\vartheta'}\mathcal{P}\left[\frac{1}{r'r}\frac{\alpha^pG^p}{n(n+1)}\right], \tag{B60}$$

$$g^{hj}_{\vartheta\varphi'} = \partial_\vartheta \partial_{\vartheta'} \mathcal{P}\left[\frac{1}{r'r}\frac{\alpha^t G^t}{n(n+1)}\right] + \frac{1}{\sin\vartheta}\frac{1}{\sin\vartheta'}\partial_\varphi \partial_{\varphi'} \mathcal{P}\left[\frac{1}{r'r}\frac{\alpha^p G^p}{n(n+1)}\right], \tag{B61}$$

$$g^{hj}_{\varphi\varphi'} = \frac{1}{\sin\vartheta}\partial_\varphi \partial_{\vartheta'} \mathcal{P}\left[\frac{1}{r'r}\frac{\alpha^t G^t}{n(n+1)}\right] - \frac{1}{\sin\vartheta'}\partial_\vartheta \partial_{\varphi'} \mathcal{P}\left[\frac{1}{r'r}\frac{\alpha^p G^p}{n(n+1)}\right], \tag{B62}$$

$$g^{hj}_{\vartheta r'} = \frac{1}{\sin\vartheta}\partial_\varphi \mathcal{P}\left[\frac{1}{r'^2 r}\frac{\alpha^p \beta^p G^p}{\sigma_0(r')}\right], \tag{B63}$$

$$g^{hj}_{\varphi r'} = -\partial_\vartheta \mathcal{P}\left[\frac{1}{r'^2 r}\frac{\alpha^p \beta^p G^p}{\sigma_0(r')}\right], \tag{B64}$$

$$g^{hj}_{r\vartheta'} = \frac{1}{\sin\vartheta'}\partial_{\varphi'} \mathcal{P}\left[\frac{1}{r'r^2}\frac{G^t}{i\omega\mu_0}\right], \tag{B65}$$

$$g^{hj}_{r\varphi'} = -\partial_{\vartheta'} \mathcal{P}\left[\frac{1}{r'r^2}\frac{G^t}{i\omega\mu_0}\right], \tag{B66}$$

$$g^{hj}_{rr'} = 0. \tag{B67}$$

Note that in eqs (B50)–(B67) $G^{t(p)} \equiv G^{t(p)}(n, r, r')$, $\alpha^{t(p)} \equiv \alpha^{t(p)}(n, r, r')$ and $\beta^{t(p)} \equiv \beta^{t(p)}(n, r, r')$. Final remark here is that some entries of G^{hj}_{1D} are written with errors both in Kuvshinov *et al.* (2002) and in Kuvshinov (2008).

APPENDIX C: GREEN'S TENSOR G^{eh}_{1D}

In this Appendix, we present the explicit forms of 3 × 3 tensor 'magnetic-to-electric' Green's functions, G^{eh}_{1D}. These tensor functions are needed to calculate the misfit gradient (Section 3.1) and they allow one to calculate the electric field that obeys Maxwell's equations

$$\nabla \times \mathbf{H}(\mathbf{r}) = \sigma_0(r)\mathbf{E}(\mathbf{r}), \tag{C1}$$

$$\nabla \times \mathbf{E}(\mathbf{r}) = i\omega\mu_0 \mathbf{H}(\mathbf{r}) + \mathbf{h}(\mathbf{r}), \tag{C2}$$

in the following integral form

$$\mathbf{E}(r, \vartheta, \varphi) = \int_V G^{eh}_{1D}(r, r', \vartheta, \vartheta', \varphi - \varphi')\mathbf{h}(r', \vartheta', \varphi')\, dv'. \tag{C3}$$

Here V is a 3-D volume occupied by magnetic source $\mathbf{h}$, and

$$G^{eh}_{1D} = \mathbf{e}_\vartheta g^{eh}_{\vartheta\vartheta'}\mathbf{e}_{\vartheta'} + \mathbf{e}_\vartheta g^{eh}_{\vartheta\varphi'}\mathbf{e}_{\varphi'} + \cdots + \mathbf{e}_r g^{eh}_{rr'}\mathbf{e}_{r'}. \tag{C4}$$

Applying the same formalism as in Appendix B we arrive to the following expressions for horizontal and radial components of the electrical field

$$\begin{aligned}\mathbf{E}_\tau(r, \vartheta, \varphi) = &\int_\Omega \int_0^\infty (\mathbf{e}_r \times \nabla_\perp)\left\{\left[\nabla'_\perp \mathcal{P}\left[\frac{r'}{r}\frac{\beta^t(n, r, r')G^t(n, r, r')}{n(n+1)}\right]\right] \cdot \mathbf{h}_\tau(r', \vartheta', \varphi')\right\} dr' d\Omega' \\ &- \int_\Omega \int_0^\infty \nabla_\perp \left\{\left[(\mathbf{e}_{r'} \times \nabla'_\perp)\mathcal{P}\left[\frac{r'}{r}\frac{\beta^p(n, r, r')G^p(n, r, r')}{n(n+1)}\right]\right] \cdot \mathbf{h}_\tau(r', \vartheta', \varphi')\right\} dr' d\Omega' \\ &- \int_\Omega \int_0^\infty (\mathbf{e}_r \times \nabla_\perp)\left\{\mathcal{P}\left[\frac{1}{r}\frac{G^t(n, r, r')}{i\omega\mu_0}\right] h_r(r', \vartheta', \varphi')\right\} dr' d\Omega',\end{aligned} \tag{C5}$$

$$E_r(r, \vartheta, \varphi) = -\int_\Omega \int_0^\infty \left[(\mathbf{e}_{r'} \times \nabla'_\perp)\mathcal{P}\left[\frac{\alpha^p(n, r, r')\beta^p(n, r, r')G^p(n, r, r')}{\sigma_0(r)r^2}\right]\right] \cdot \mathbf{h}_\tau(r', \vartheta', \varphi')\, dr' d\Omega'. \tag{C6}$$

Now from eqs (C5) and (C6) we write the expressions for elements $g^{eh}_{\vartheta\vartheta'}, g^{eh}_{\vartheta\varphi'}, \ldots, g^{eh}_{rr'}$ of eq. (C4)

$$g^{eh}_{\vartheta\vartheta'} = -\frac{1}{\sin\vartheta}\partial_\varphi \partial_{\vartheta'} P\left[\frac{1}{rr'}\frac{\beta^t G^t}{n(n+1)}\right] + \frac{1}{\sin\vartheta'}\partial_\vartheta \partial_{\varphi'} P\left[\frac{1}{rr'}\frac{\beta^p G^p}{n(n+1)}\right], \tag{C7}$$

$$g^{eh}_{\vartheta\varphi'} = -\frac{1}{\sin\vartheta}\frac{1}{\sin\vartheta'}\partial_\varphi \partial_{\varphi'} P\left[\frac{1}{rr'}\frac{\beta^t G^t}{n(n+1)}\right] - \partial_\vartheta \partial_{\vartheta'} P\left[\frac{1}{rr'}\frac{\beta^p G^p}{n(n+1)}\right], \tag{C8}$$

$$g^{eh}_{\vartheta r'} = \frac{1}{\sin\vartheta}\partial_\varphi P\left[\frac{1}{r'^2 r}\frac{G^t}{i\omega\mu_0}\right], \tag{C9}$$

$$g^{eh}_{\varphi\vartheta'} = \partial_\vartheta \partial_{\vartheta'} P\left[\frac{1}{rr'}\frac{\beta^t G^t}{n(n+1)}\right] + \frac{1}{\sin\vartheta}\frac{1}{\sin\vartheta'}\partial_\varphi \partial_{\varphi'} P\left[\frac{1}{rr'}\frac{\beta^p G^p}{n(n+1)}\right], \tag{C10}$$

$$g^{eh}_{\varphi\varphi'} = \frac{1}{\sin\vartheta'}\partial_\vartheta \partial_{\varphi'} P\left[\frac{1}{rr'}\frac{\beta^t G^t}{n(n+1)}\right] - \frac{1}{\sin\vartheta}\partial_\varphi \partial_{\vartheta'} P\left[\frac{1}{rr'}\frac{\beta^p G^p}{n(n+1)}\right], \tag{C11}$$

$$g^{eh}_{\varphi r'} = -\partial_\vartheta P\left[\frac{1}{r'^2 r}\frac{G^t}{i\omega\mu_0}\right], \tag{C12}$$

$$g^{eh}_{r\vartheta'} = \frac{1}{\sin\vartheta'}\partial_{\varphi'} P\left[\frac{1}{r^2 r'}\frac{\alpha^p\beta^p G^p}{\sigma_0(r)}\right], \tag{C13}$$

$$g^{eh}_{r\varphi'} = -\partial_{\vartheta'} P\left[\frac{1}{r^2 r'}\frac{\alpha^p\beta^p G^p}{\sigma_0(r)}\right], \tag{C14}$$

$$g^{eh}_{rr'} = 0. \tag{C15}$$

Note that one can verify that due to the reciprocity principle (*cf.* Pankratov & Kuvshinov 2010b, Appendix A)

$$G^{eh}_{1\mathrm{D}}(\mathbf{r},\mathbf{r}')^T = G^{hj}_{1\mathrm{D}}(\mathbf{r}',\mathbf{r}). \tag{C16}$$

APPENDIX D: DERIVATION OF SCALAR GREEN'S FUNCTIONS

The scalar Green's functions $G^{t(p)}(n,r,r')$ are continuous solutions of the equation

$$\partial_r\left[\frac{1}{p^{t(p)}(r)}\partial_r G^{t(p)}(n,r,r')\right] = q^{t(p)}(r)G^{t(p)}(n,r,r') + \delta(r-r'), \tag{D1}$$

with the imposed boundary conditions: $G^{t(p)}(n,r,r') \to 0$ when $r \to 0$ and $r \to \infty$. The coefficients for the two modes ('t' and 'p') are defined in eq. (B20) and eq. (B21), respectively. From eq. (D1) we obtain the following matching condition

$$\frac{1}{p(r'+0)}\partial_r G(n,r'+0,r') = \frac{1}{p(r'-0)}\partial_r G(n,r'-0,r') + 1. \tag{D2}$$

Here and later in this section we will omit superscripts 't' and 'p' for the simplicity of presentation. By fixing r' we write

$$G(n,r,r') = \begin{cases} v^u(n,r), \ r > r' \\ v^l(n,r), \ r < r' \end{cases}, \tag{D3}$$

where functions $v^u(n,r)$ and $v^l(n,r)$ satisfy the equation

$$\partial_r\left[\frac{1}{p(r)}\partial_r v^{l(u)}(n,r)\right] = q(r)v^{l(u)}(n,r), \tag{D4}$$

and where $v^u(n,r) \to 0$, when $r \to \infty$, and $v^l(n,r) \to 0$, when $r \to 0$. We introduce further 'lower', Y^l, and 'upper', Y^u, admittances as follows

$$Y^l(n,r) = \frac{1}{p(r)}\frac{\partial_r v^l(n,r)}{v^l(n,r)}, \quad Y^u(n,r) = -\frac{1}{p(r)}\frac{\partial_r v^u(n,r)}{v^u(n,r)}. \tag{D5}$$

Using eq. (D5) we write

$$v^l(n,r) = v^l(n,r')\exp\left[\int_{r'}^{r} p(\xi)Y^l(n,\xi)\,\mathrm{d}\xi\right], \quad v^u(n,r) = v^u(n,r')\exp\left[-\int_{r'}^{r} p(\xi)Y^u(n,\xi)\,\mathrm{d}\xi\right]. \tag{D6}$$

Then substituting eq. (D6) into eq. (D3) and using eq. (D2) we obtain

$$\frac{1}{p(r'+0)}\partial_r v^u(n,r'+0) = \frac{1}{p(r'-0)}\partial_r v^l(n,r'-0) + 1. \tag{D7}$$

Noting the continuity of $G(n,r,r')$ with respect to r we write

$$v^u(n,r'+0) = v^u(n,r') = v^l(n,r') = v^l(n,r'-0). \tag{D8}$$

Then using eq. (D5) we represent $v^u(n,r')$ and $v^l(n,r')$ as

$$v^u(n,r') = v^l(n,r') = -\frac{1}{Y^l(n,r') + Y^u(n,r')}. \tag{D9}$$

And finally from eqs (D3), (D6)–(D9) we write the explicit form of scalar Green's function as

$$G(n,r,r') = -\frac{1}{Y^l(n,r') + Y^u(n,r')} \cdot \exp\left[\int_{r'}^{r} p(n,\xi)\alpha(n,\xi,r')\,\mathrm{d}\xi\right], \tag{D10}$$

where the spectral function α is defined as

$$\alpha(n,r,r') = \begin{cases} -Y^u(n,r), & r > r' \\ Y^l(n,r), & r < r' \end{cases}. \tag{D11}$$

APPENDIX E: CALCULATION OF ADMITTANCES

To calculate the admittances $Y^{l,t(p)}(n, r)$ and $Y^{u,t(p)}(n, r)$ we assume that the radially symmetric reference section consists of N layers $\{r_{k+1} < r \le r_k\}_{k=1,2,\ldots,N}$. We construct the set $\{r_k\}_{k=1,2,\ldots,N}$ in such a way that it includes all levels r_j, where we will calculate the admittances and the Green's scalar functions.We assume that within each layer the conductivity varies as

$$\sigma_o(r) = \sigma_k\left(\frac{r_k}{r}\right)^2, \quad r_{k+1} < r \le r_k, \tag{E1}$$

where $r_1 = a$, $r_{N+1} = 0$, σ_k is an appropriate constant. Distribution (E1) (*cf.* Rokityansky 1982; Fainberg *et al.* 1990) is chosen to make recurrent calculations of $Y^{l,t(p)}(n, r)$ and $Y^{u,t(p)}(n, r)$ for any n as accurate and stable as possible. Because N can be taken as large as necessary, the distribution (E1) allows for the approximation of any radially symmetric conductivity distribution. Let us show, with an example of $Y^{l,p}(n, r)$, how these recurrences are derived.

According to eq. (B21) and using eq. (E1), eq. (D4) for $\nu^{l,p}$ within kth layer is written as

$$\frac{\partial^2}{\partial r^2}\nu^{l,p}(n,r) - \frac{n(n+1) - \mathrm{i}\omega\mu_0\sigma_k r_k^2}{r^2}\nu^{l,p}(n,r) = 0. \tag{E2}$$

The solution of eq. (E2) has the form

$$\nu^{l,p}(n,r) = A_k^{l,p}\left(\frac{r_{k+1}}{r}\right)^{b_k^-} + B_k^{l,p}\left(\frac{r}{r_{k+1}}\right)^{b_k^+}, \tag{E3}$$

where

$$b_k^- = b_k - \frac{1}{2}, \quad b_k^+ = b_k + \frac{1}{2}, \quad b_k = \left\{\left(n+\frac{1}{2}\right)^2 - \mathrm{i}\omega\mu_0\sigma_k r_k^2\right\}^{\frac{1}{2}}. \tag{E4}$$

From eq. (E3) we get

$$\partial_r\nu^{l,p}(n,r) = \frac{-b_k^- A_k^{l,p}}{r_{k+1}}\left(\frac{r_{k+1}}{r}\right)^{b_k^-+1} + \frac{b_k^+ B_k^{l,p}}{r_{k+1}}\left(\frac{r}{r_{k+1}}\right)^{b_k^+-1}. \tag{E5}$$

Substituting eq. (E3) and eq. (E5) into eq. (D5), taking into account eq. (B21), we obtain

$$Y^{l,p}(n,\omega,r) = \frac{\sigma_k r_k^2}{b_k^+ b_k^-}\frac{-\frac{b_k^- C_k^{l,p}}{r_{k+1}}\left(\frac{r_{k+1}}{r}\right)^{b_k^-+1} + \frac{b_k^+}{r_{k+1}}\left(\frac{r}{r_{k+1}}\right)^{b_k^+-1}}{C_k^{l,p}\left(\frac{r_{k+1}}{r}\right)^{b_k^-} + \left(\frac{r}{r_{k+1}}\right)^{b_k^+}}, \tag{E6}$$

where $C_k^{l,p} = \frac{A_k^{l,p}}{B_k^{l,p}}$. By setting $r = r_{k+1}$ in eq. (E6) we obtain for $C_k^{l,p}$

$$C_k^{l,p} = \frac{\frac{\sigma_k r_k^2}{b_k^- r_{k+1}} - Y_{k+1}^{l,p}}{\frac{\sigma_k r_k^2}{b_k^+ r_{k+1}} + Y_{k+1}^{l,p}}, \tag{E7}$$

where $Y_{k+1}^{l,p} \equiv Y^{l,p}(n, \omega, r_{k+1})$. Substituting eq. (E7) into eq. (E6) we finally have the recurrence

$$Y_k^{l,p} \equiv Y^{l,p}(n,\omega,r_k) = g_k\frac{Y_{k+1}^{l,p}(b_k - 0.5\tau_k) - g_l\eta_k\tau_k}{g_k\eta_k(b_k + 0.5\tau_k) - b_k^+ b_k^-\tau_k Y_{k+1}^{p,l}}, \quad k = N-1, N-2, \ldots, 1, \tag{E8}$$

where

$$\eta_k = \frac{r_k}{r_{k+1}}, \quad \tau_k = \frac{1-\zeta_k}{1+\zeta_k}, \quad \zeta_k = \eta_k^{2b_k}, \quad g_k = \sigma_k r_k, \tag{E9}$$

and

$$Y_N^{l,p} = \frac{\sigma_N r_N}{b_N^-}. \tag{E10}$$

Deriving eq. (E8) we used continuity of admittance at the boundaries of the spherical layers. In addition, while deriving eq. (E10) we used the fact that $A_N^{p,l} = 0$, what follows from boundary condition $v^{l,p} \to 0$, when $r \to 0$. In a similar way we derive the recurrences for $Y^{u,p}$, $Y^{l,t}$, $Y^{u,t}$

$$Y_k^{l,t} = \frac{1}{q_k} \frac{q_{k+1} Y_{k+1}^{l,t}(b_k - 0.5\tau_k) + b_k^+ b_k^- \tau_k}{(b_k + 0.5\tau_k) + q_{k+1}\tau_k Y_{k+1}^{l,t}}, \quad k = N-1, N-2, \ldots, 1, \quad Y_N^{l,t} = -\frac{b_N^+}{q_N}, \tag{E11}$$

$$Y_{k+1}^{u,t} = \frac{1}{q_{k+1}} \frac{q_k Y_k^{u,t}(b_k + 0.5\tau_k) + b_k^+ b_k^- \tau_k}{(b_k - 0.5\tau_k) + q_k \tau_k Y_k^{u,t}}, \quad k = 1, 2, \ldots, N-1, \quad Y_1^{u,t} = -\frac{b_1^-}{q_1}, \tag{E12}$$

$$Y_{k+1}^{u,p} = g_k \eta_k \frac{Y_k^{u,p}(b_k + 0.5\tau_k) - g_k \tau_k}{g_k(b_k - 0.5\tau_k) - b_k^+ b_k^- \tau_k Y_k^{u,p}}, \quad k = 1, 2, \ldots, N-1, \quad Y_1^{u,p} = \frac{\sigma_1 r_1}{b_1^+}, \tag{E13}$$

where

$$q_k = \mathrm{i}\omega\mu_0 r_k. \tag{E14}$$

APPENDIX F: CALCULATION OF SCALAR GREEN FUNCTIONS

Finally, we show how to calculate $G^{t(p)}(n, r, r')$ when $r \neq r'$. Let us consider the calculation of $G^t(n, r_i, r_j)$ when $r_i \leq r_j$. From eqs (D10) and (D11) it follows that $G^t(n, r_i, r_j)$ can be written as

$$G^t(n, r_i, r_j) = -\frac{1}{Y_j^{l,t} + Y_j^{u,t}} \prod_{k=j}^{i} F_k^t, \quad r_i \leq r_j, \tag{F1}$$

where F_k^t is defined as

$$F_k^t = \exp\left(\int_{r_{k+1}}^{r_k} \mathrm{i}\omega\mu_0 Y^{l,t}(n, r)\, \mathrm{d}r \right), \tag{F2}$$

and $Y^{l,t}$ (in analogy with $Y^{l,p}$) has the form

$$Y^{l,t}(n, r) = -\frac{1}{\mathrm{i}\omega\mu_0} \frac{-\frac{b_k^- C_k^{l,t}}{r_{k+1}} \left(\frac{r_{k+1}}{r}\right)^{b_k^- + 1} + \frac{b_k^+}{r_{k+1}} \left(\frac{r}{r_{k+1}}\right)^{b_k^+ - 1}}{C_k^{l,t} \left(\frac{r_{k+1}}{r}\right)^{b_k^-} + \left(\frac{r}{r_{k+1}}\right)^{b_k^+}}. \tag{F3}$$

Substituting eq. (F3) into eq. (F2) we derive

$$\begin{aligned} \int_{r_{k+1}}^{r_k} \mathrm{i}\omega\mu_0 Y^{l,t}(n, r)\, dr &= \frac{1}{r_{k+1}} \int_{r_{k+1}}^{r_k} \frac{b_k^- C_k^{l,t} - b_k^+ \left(\frac{r}{r_{k+1}}\right)^{2b_k}}{\left(\frac{r}{r_{k+1}}\right)\left(C_k^{l,t} + \left(\frac{r}{r_{k+1}}\right)^{2b_k}\right)} \mathrm{d}r = \\ &= \frac{1}{b_k} \int_1^{\zeta_k} \frac{C_k^{l,t} b_k^- - b_k^+ \gamma_k}{\gamma_k (C_k^{l,t} + \gamma_k)} \mathrm{d}\gamma_k = \ln\left(\frac{C_k^{l,t} + 1}{C_k^{l,t} + \gamma_k} \eta_k^{b_k^-} \right). \end{aligned} \tag{F4}$$

Although integrating we used the change of variables, $\gamma_k = \eta^{2b_k}$, where $\eta = \frac{r}{r_{k+1}}$ and tabular integrals $\int \frac{dx}{a+bx} = \frac{1}{b} ln(a + bx)$, $\int \frac{dx}{x(a+bx)} = -\frac{1}{a} ln\left(\frac{a+bx}{x}\right)$. Setting further in eq. (F3) $r = r_{k+1}$ we obtain for $C_k^{l,t}$

$$C_k^{l,t} = \frac{b_k^+ + \mathrm{i}\omega\mu_0 Y_{k+1}^{l,t}}{b_k^- - \mathrm{i}\omega\mu_0 Y_{k+1}^{l,t}}. \tag{F5}$$

Substituting eq. (F5) into eq. (F4) and then eq. (F4) into eq. (F2) we get for F_k^t

$$F_k^t = \frac{1}{1 + \zeta_k} \frac{2b_k \eta_k^{b_k^-}}{(b_k + 0.5\tau_k) + q_k \tau_k Y_{k+1}^{l,t}}. \tag{F6}$$

In a similar way we obtain the expressions for another mode

$$G^p(n, r_i, r_j) = -\frac{1}{Y_j^{l,p} + Y_j^{u,p}} \prod_{k=j}^{i} F_k^p, \quad r_i \leq r_j, \tag{F7}$$

where

$$F_k^p = \frac{1}{1 + \zeta_k} \frac{2g_k b_k \eta_k^{b_k^-}}{g_k \eta_k (b_k + 0.5\tau_k) - b_k^+ b_k^- \tau_k Y_{k+1}^{l,p}}. \tag{F8}$$

Due to symmetry of scalar Green's functions, $G^{t(p)}(n, r, r') = G^{t(p)}(n, r', r)$, one derives the results for $r_i > r_j$.

APPENDIX G: REPRESENTATION OF $\mathbf{B}^e$ VIA EQUIVALENT SHEET CURRENT

The results presented here will be used in Appendix H. It is known that in the source-free (and insulating) region, the magnetic field **B** can be represented via the scalar magnetic potential V

$$\mathbf{B} = \mu_0 \mathbf{H} = -\nabla V. \tag{G1}$$

Because magnetic field is solenoidal

$$\nabla \cdot \mathbf{B} = 0, \tag{G2}$$

potential V satisfies Laplace's equation

$$\Delta V = 0. \tag{G3}$$

The general solution of Laplace's equation in spherical coordinates in this region is given by

$$V = a \sum_{n,m} \left[\epsilon_n^m \left(\frac{r}{a}\right)^n + \iota_n^m \left(\frac{a}{r}\right)^{n+1} \right] S_n^m(\vartheta, \varphi), \tag{G4}$$

where $\epsilon_n^m \equiv \epsilon_n^m(\omega)$ and $\iota_n^m \equiv \iota_n^m(\omega)$ are the complex-valued expansion coefficients of inducing (external) and induced (internal) parts of the potential. Using eqs (G1) and (G4) one can write magnetic field, **B**, in the form

$$\mathbf{B} = \mathbf{B}^e + \mathbf{B}^i, \tag{G5}$$

where

$$\mathbf{B}^e = -\nabla \left\{ a \sum_{n,m} \epsilon_n^m \left(\frac{r}{a}\right)^n S_n^m(\vartheta, \varphi) \right\}, \tag{G6}$$

$$\mathbf{B}^i = -\nabla \left\{ a \sum_{n,m} \iota_n^m \left(\frac{a}{r}\right)^{n+1} S_n^m(\vartheta, \varphi) \right\}. \tag{G7}$$

Let us introduce a spherical, infinitely thin shell of radius b and assume that the shell is surrounded by the insulator. We also assume that the current system flows in the shell, and therefore is described by the sheet current density, $\mathbf{J}_\tau^{\rm ext}$. In the region above the shell $r > b$ the source is seen as internal, producing a magnetic field of the form of eq. (G7). Below the shell $r < b$ the source is seen as external, producing a field with a magnetic potential of the form of eq. (G6). However, because **B** is solenoidal, one can obtain (using Gauss theorem) that the radial component, B_r, is continuous across the shell, and thus

$$B_r^i\big|_{r=b} = B_r^e\big|_{r=b}. \tag{G8}$$

Substituting expressions for B_r^e and B_r^i from eqs (G6) and (G7) into eq. (G8) we find that coefficients ϵ_n^m and ι_n^m are connected via relation

$$\iota_n^m = -\frac{n}{n+1} \left(\frac{b}{a}\right)^{2n+1} \epsilon_n^m. \tag{G9}$$

In contrast to the radial component of magnetic field which is continuous across the shell, horizontal components have a jump across the shell

$$\mathbf{J}_\tau^{\rm ext} = \frac{\delta(r-b)}{\mu_0} \mathbf{e}_r \times \left(\mathbf{B}_\tau^+ - \mathbf{B}_\tau^-\right), \tag{G10}$$

which follows from Ampere′s law. Here

$$\mathbf{B}_\tau^+ = \mathbf{B}_\tau|_{r\to b+0} = \mathbf{B}_\tau^i|_{r=b}, \tag{G11}$$

$$\mathbf{B}_\tau^- = \mathbf{B}_\tau|_{r\to b-0} = \mathbf{B}_\tau^e|_{r=b}. \tag{G12}$$

Substituting expressions for $\mathbf{B}_\tau^e$ and $\mathbf{B}_\tau^i$ from eqs (G11) and (G12) into eq. (G10), and using eqs (G6)–(G7) and relation (G9) we express $\mathbf{J}_\tau^{\rm ext}$ via the external coefficients ϵ_n^m as

$$\mathbf{J}_\tau^{\rm ext} = \frac{\delta(r-b)}{\mu_0} \sum_{n,m} \frac{2n+1}{n+1} \epsilon_n^m \left(\frac{b}{a}\right)^{n-1} \mathbf{e}_r \times \nabla_\perp S_n^m(\vartheta, \varphi). \tag{G13}$$

Thus, the currents in the form of eq. (G13) flowing in a shell $r = b \geq a$ (embedded in an insulator) produce exactly the external magnetic field $\mathbf{B}^e$ below the shell in the region $a \leq r < b$.

APPENDIX H: REPRESENTATION OF EM FIELD IN 1-D CONDUCTIVITY MODEL VIA EXTERNAL COEFFICIENTS

In Appendix G, we discussed a representation of our impressed (magnetospheric) source in the form of a SHE of an equivalent sheet current, $\mathbf{J}^{\rm ext}_\tau$. Now we obtain the representation for $\mathbf{E}^0$ and $\mathbf{H}^0$ (*cf.* eqs 13–12) via $\mathbf{J}^{\rm ext}_\tau$ (and thus via inducing coefficients ϵ^m_n). Substituting eq. (G13) into eq. (B34), then the resulting expression into eq. (B30), by accounting eqs (B7) and (B9), and rearranging operations of integration and summation, we write the SHE for the horizontal electric field, $\mathbf{E}^0_\tau$, in the following form

$$\mathbf{E}^0_\tau(r,\vartheta,\varphi)=\frac{1}{\mu_0}\frac{b}{r}\sum_{n,m}\frac{2n+1}{n+1}\epsilon^m_n\left(\frac{b}{a}\right)^{n-1}G^t(n,r,b)\,\mathbf{e}_r\times\nabla_\perp S^m_n(\vartheta,\varphi). \tag{H1}$$

Because the sheet current is horizontal and, moreover, contains only one ('t') mode, then

$$E^0_r(r,\vartheta,\varphi)=0. \tag{H2}$$

In a similar way, using eqs (B6), (B7), (B13), (B14), (B18) and (B32) we write SHE for the magnetic field, $\mathbf{H}^0$, as

$$H^0_r(r,\vartheta,\varphi)=-\frac{1}{{\rm i}\omega\mu_0}\frac{b}{\mu_0 r^2}\sum_{n,m}(2n+1)n\epsilon^m_n\left(\frac{b}{a}\right)^{n-1}G^t(n,r,b)S^m_n(\vartheta,\varphi), \tag{H3}$$

$$\mathbf{H}^0_\tau(r,\vartheta,\varphi)=\frac{1}{\mu_0}\frac{b}{r}\sum_{n,m}\frac{2n+1}{n+1}\epsilon^m_n\left(\frac{b}{a}\right)^{n-1}\alpha^t(n,r,b)G^t(n,r,b)\nabla_\perp S^m_n(\vartheta,\varphi). \tag{H4}$$

Let us obtain expressions for electric and magnetic field at the surface of the Earth. Assume that $\mathbf{J}^{\rm ext}_\tau$ flows just above the Earth's surface, that is, at $b=a+$. From eqs (D10), (E4), (E11), (E12) and (E14) we then have

$$G^t(n,a,a+)=-\frac{{\rm i}\omega\mu_0 a}{{\rm i}\omega\mu_0 a Y^{l,t}_1-n}, \tag{H5}$$

and from eq. (D11)

$$\alpha^t(n,a,a+)=Y^{l,t}_1. \tag{H6}$$

Using eqs (H5) and (H6) we finally derive expressions for the electric and magnetic fields on the surface of the Earth

$$\mathbf{E}^0_\tau(a,\vartheta,\varphi)=-\frac{1}{\mu_0}\sum_{n,m}\frac{2n+1}{n+1}\epsilon^m_n\frac{{\rm i}\omega\mu_0 a}{{\rm i}\omega\mu_0 a Y^{l,t}_1-n}\,\mathbf{e}_r\times\nabla_\perp S^m_n(\vartheta,\varphi), \tag{H7}$$

$$H^0_r(a,\vartheta,\varphi)=\frac{1}{\mu_0}\sum_{n,m}(2n+1)n\epsilon^m_n\frac{1}{{\rm i}\omega\mu_0 a Y^{l,t}_1-n}S^m_n(\vartheta,\varphi), \tag{H8}$$

$$\mathbf{H}^0_\tau(a,\vartheta,\varphi)=-\frac{1}{\mu_0}\sum_{n,m}\frac{2n+1}{n+1}\epsilon^m_n\frac{{\rm i}\omega\mu_0 a Y^{l,t}_1}{{\rm i}\omega\mu_0 a Y^{l,t}_1-n}\nabla_\perp S^m_n(\vartheta,\varphi). \tag{H9}$$

Note that the C-responses at the Earth's surface, $C_n(\omega,a)$, are connected to $Y^{l,t}_1(n,\omega)\equiv Y^{l,t}(n,\omega,a)$ as

$$C_n(\omega,a)=-\frac{1}{{\rm i}\omega\mu_0 Y^{l,t}_1(n,\omega)}. \tag{H10}$$

If we assume that ϑ and φ correspond to geomagnetic coordinate system then C_1 gives the response discussed in Section 2.2.

A final remark concerns the connection between $Y^{l,t}_1(n,\omega)$ and $Q_n(\omega)$ which is defined as

$$Q_n(\omega)=\frac{\epsilon^m_n(\omega)}{\iota^m_n(\omega)}. \tag{H11}$$

Note, that in the case of a 1-D conductivity distribution this ratio is independent of m. With the use of eq. (H11) and eqs (G5)–(G7) the magnetic field at the surface of the Earth can be written in an alternative manner as

$$H^0_r(a,\vartheta,\varphi)=-\frac{1}{\mu_0}\sum_{n,m}\epsilon^m_n\big(n-(n+1)Q_n\big)S^m_n(\vartheta,\varphi), \tag{H12}$$

$$\mathbf{H}^0_\tau(a,\vartheta,\varphi)=-\frac{1}{\mu_0}\sum_{n,m}\epsilon^m_n\big(1+Q_n\big)\nabla_\perp S^m_n(\vartheta,\varphi). \tag{H13}$$

Equating eq. (H12) with eq. (H8) (or eq. H13 with eq. H9) one can deduce that

$$Q_n(\omega)=\frac{n}{n+1}\frac{{\rm i}\omega\mu_0 a Y^{l,t}_1(n,\omega)+n+1}{{\rm i}\omega\mu_0 a Y^{l,t}_1(n,\omega)-n}. \tag{H14}$$